arXiv:1609.02152v1 [astro-ph.SR] 7 Sep 2016

Ultra-deep GEMINI near-infrared observations of the bulge globular cluster NGC 6624[1]

S. Saracino[1,2], E. Dalessandro[1,2], F. R. Ferraro[1], D. Geisler[3], F. Mauro[4,3], B. Lanzoni[1], L. Origlia[2], P. Miocchi[1], R. E. Cohen[3], S. Villanova[3], C. Moni Bidin[5]

September 7, 2016

ABSTRACT

We used ultra-deep J and K_s images secured with the near-infrared GSAOI camera assisted by the multi-conjugate adaptive optics system GeMS at the GEMINI South Telescope in Chile, to obtain a (K_s, $J - K_s$) color-magnitude diagram (CMD) for the bulge globular cluster NGC 6624. We obtained the deepest and most accurate near-infrared CMD from the ground for this cluster, by reaching $K_s \sim 21.5$, approximately 8 magnitudes below the horizontal branch level. The entire extension of the Main Sequence (MS) is nicely sampled and at $K_s \sim 20$ we detected the so-called MS "knee" in a purely near-infrared CMD. By taking advantage of the exquisite quality of the data, we estimated the absolute age of NGC 6624 ($t_{age} = 12.0 \pm 0.5$ Gyr), which turns out to be in good agreement with previous studies in the literature. We also analyzed the luminosity and mass functions of MS stars down to M $\sim$ 0.45 $M_\odot$ finding evidence of a significant increase of low-mass stars at increasing distances from the cluster center. This is a clear signature of mass segregation, confirming that NGC 6624 is in an advanced stage of dynamical evolution.

Subject headings: Globular Clusters: Individual (NGC 6624) - Instrumentation: adaptive optics - Technique: photometry

[1]Dipartimento di Fisica e Astronomia, Università di Bologna, Viale Berti Pichat 6/2, I-40127 Bologna, Italy - *sara.saracino@unibo.it*

[2]INAF - Osservatorio Astronomico di Bologna, via Ranzani 1, I-40127 Bologna, Italy

[3]Departamento de Astronomía, Universidad de Concepción, Casilla 160-C, Concepción, Chile

[4]Millennium Institute of Astrophysics, Chile

[5]Instituto de Astronomía, Universidad Católica del Norte, Av. Angamos 0610, Antofagasta, Chile

[1]Based on observations obtained at the Gemini Observatory, which is operated by the Association of

1. Introduction

Globular Clusters (GCs) are complex systems hosting $10^4 - 10^6$ gravitationally bound stars, distributed with an approximately spherical geometry. In the central regions of these stellar systems, where stars are forced to live in an extremely dense environment, the probability of stellar encounters is highly enhanced. Such collisions lead to the formation of peculiar objects like Cataclysmic Variables, Low Mass X-ray Binaries (LMXBs), Millisecond Pulsars and Blue Straggler Stars (e.g. Bailyn 1992; Paresce et al. 1992; Ferraro et al. 2001, 2009a, 2012; Ransom et al. 2005; Pooley & Hut 2006) and they influence the time scales on which mass segregation, core collapse and other dynamical processes occur (Meylan & Heggie 1997).

The large stellar concentration in the central regions of high density GCs prohibited to resolve individual stars for many years, until the launch of Hubble Space Telescope (HST), which allowed exquisite resolution over a relatively large (a few square arcmin) field of view (FOV) mainly in the optical bands. The investigation of the stellar content of GCs in the bulge of the Galaxy has the additional complication of the presence of thick clouds of dust along the line of sight that almost totally absorb the optical light, and/or the presence of a heavy field star contamination. The exploration of such clusters requires near-infrared (NIR) observations (e.g., Ferraro et al. 2000, 2009b; Valenti et al. 2004a, 2007; Origlia et al. 1997, 2011), a wavelength range where the foreground extinction significantly drops. The observations of such stellar systems in the NIR have tremendously improved with the advent of instrumentation assisted by the new adaptive optics (AO) facilities. These systems, in fact, mainly work in the NIR, where the spatial and temporal coherence of the corrugated wavefront is larger (Davies & Kasper 2012), and they are able to compensate the blurriness of the astronomical images due to the Earth's atmosphere by using one or more deformable mirrors and, as reference, natural and/or laser guide stars.

The Gemini South Telescope, on Cerro Pachón in Chile, currently is the only facility equipped with a Multi-conjugate Adaptive Optics System (named GeMS), which uses three natural guide stars, a constellation of five laser guide stars and two deformable mirrors conjugated at the ground and at an altitude of 9 km (see Rigaut et al. 2014; Neichel et al. 2014). This allows GeMS to (almost) reach the diffraction limit of the telescope. By

---

Universities for Research in Astronomy, Inc., under a cooperative agreement with the NSF on behalf of the Gemini partnership: the National Science Foundation (United States), the National Research Council (Canada), CONICYT (Chile), the Australian Research Council (Australia), Ministério da Ciência, Tecnologia e Inovação (Brazil) and Ministerio de Ciencia, Tecnología e Innovación Productiva (Argentina). Based on observations gathered with ESO-VISTA telescope (program ID 179.B-2002).

exploiting the unprecedented capabilities of this system, which works in combination with the NIR high-resolution camera Gemini South Adaptive Optics Imager (GSAOI), we started an observing campaign of a set of GCs located in the Galactic bulge. After the encouraging results obtained for Liller 1 (Saracino et al. 2015), a heavily obscured cluster located very close to the Galactic plane and center, here we present the results for NGC 6624. This GC is located just at the edge of the inner bulge, at a distance of 7.9 Kpc from Earth (Harris 1996, 2010 edition) and it is characterized by only a moderate foreground extinction for a bulge GC, $E(B-V) = 0.28$ (Valenti et al. 2004a; Harris 1996, 2010 edition). These features also make NGC 6624 an ideal target to investigate the sky performance of the GeMS+GSAOI system.

NGC 6624 is a well-studied cluster, but mainly in the optical bands (see Sarajedini et al. 2007; Dalessandro et al. 2014). In the NIR it was observed with the following instruments:

(i) IRCAM, mounted at the 2.5 m Du Pont telescope. These observations provided the first (K_s, $J-K_s$) CMD of the cluster sampling the brightest portion of the red giant branch (RGB; see Kuchinski & Frogel 1995) down to the Horizontal Branch (HB) level.

(ii) IRAC-2 mounted at the ESO 2.2 m telescope MPI. The NIR CMD derived from these observations was deeper than the previous one, reaching the cluster sub-giant branch ($K_s \sim 17$), and thus allowing to study the RGB features (RGB bump and tip; see Valenti et al. 2004a,b, 2007; Ferraro et al. 2006b).

(iii) Within the *VISTA Variables in the Via Lactea* (hereafter VVV) survey. The NIR CMD obtained from the VVV catalog was deep enough ($K_s \sim 19$) to sample the main sequence turn-off (MS-TO) only in the external regions of the cluster (Minniti et al. 2010; Catelan et al. 2011).

NGC 6624 is quite compact and it has been catalogued as a dynamically evolved cluster, which already experienced core collapse (Trager et al. 1995). It has been found to harbour six millisecond pulsars (Lynch et al. 2012; Tam et al. 2011; Freire et al. 2011) and at least an ultra-compact LMXB (Dib et al. 2005), thus confirming that its dense environment efficiently boosts the formation of exotic objects.

In this paper we present ultra-deep NIR observations of NGC 6624 obtained by using the powerful combination of the GeMS+GSAOI devices mounted at the Gemini South Telescope. The paper is organized as follows: in Section 2 we discuss the observations and the data analysis. In Section 3 we present the CMD of the cluster. Section 4 is focused on the determination of the age of the cluster and in Section 5 we discuss the Luminosity (LF) and Mass Functions (MF) of the cluster MS. In Section 6 we present our conclusions.

2. Observations and data analysis

The data set analyzed in this work consists of a sample of high-quality J and K_s images obtained with GeMS and the NIR camera GSAOI. GSAOI has a resolution of about $0.02''$/pixels and consists of four 2048 x 2048 pixels chips, divided by gaps of about $2''$, providing a total FOV of almost $85'' \times 85''$. NGC 6624 was observed on May 24, 2013 as part of the proposal GS-2013-Q-23 (PI: D. Geisler). A total of 28 images (14 in the J and 14 in the K_s bands), with an exposure time $t_{\rm exp} = 30$ s each, was acquired during the run. To fully cover the gaps between the GSAOI chips, we adopted a dither pattern with a maximum offset of about $5''$ between two consecutive images. During the observing night the DIMM monitor on Cerro Pachón recorded excellent seeing conditions, with a Full Width at Half Maximum (FWHM) of $\sim 0.7''$. An average stellar FWHM smaller than 4 pixels ($0.08''$, close to the diffraction limit of the telescope) has been measured in all J and K_s images. Unfortunately, one J-band exposure was characterized by a significantly worse FWHM, so it was excluded from the subsequent analysis. In Figure 1 we present a two-color mosaic of K_s and J images of NGC 6624. Figure 2 shows the comparison between a central region ($10''\times 10''$) of NGC 6624 obtained with HST in the F435W filter (*left panel*) and with GeMS/GSAOI system in the K_s band (*right panel*): the spatial resolution of the AO corrected image is indeed impressive.

The data analysis was performed following the same procedure described in Saracino et al. (2015). Briefly, each individual chip[2] was analyzed independently, by using standard pre-reduction procedure, within the `IRAF`[3] environment, in order to correct for flat-field and bias and subtract the background. For this purpose, a Master Sky was obtained by combining 5 sky images per filter of a relatively empty field. In order to get accurate photometry, even in the innermost region of the cluster, we performed point-spread function (PSF) fitting by using `DAOPHOT` (Stetson 1987) of all the detected stellar sources. For each chip, we selected $\sim$ 100 bright, isolated and unsaturated stars (using `FIND` and `PHOTO`), that were used to derive the best-fit PSF model. Based on a χ^2 test, the best-fit PSF analytic models were found to be a MOFFAT function (with β=1.5; Moffat 1969) for the K_s images and a PENNY function (Penny 1976) for the J ones. We also noted that photometry significantly improves by adopting PSF models varying within the FOV. In particular we

[2]To distinguish between chips, we assigned an identification (ID) number from 1 to 4, starting from the bottom-right corner (chip 1) and proceeding clockwise.

[3]IRAF is distributed by the National Optical Astronomy Observatory, which is operated by the Association of Universities for Research in Astronomy, Inc., under cooperative agreement with the National Science Foundation.

adopted a linear dependence on the position within the frame in chip 1, and a cubic one for chips 2, 3 and 4. The selected models were then applied, using the `ALLSTAR` and `ALLFRAME` tasks (Stetson 1994), to all the sources having peak counts larger than 3σ above the local background level, thus determining the instrumental magnitudes for each star candidate in each chip. In the catalog we included only stars present in at least two images for each filter. This criterion removed most of the cosmic rays and other spurious detections and allowed to fill the gaps between the different chips of GSAOI. For each star, we homogenized the magnitudes estimated in different images, and their weighted mean and standard deviation have been finally adopted as the star mean magnitude and its related photometric error (see Ferraro et al. 1991, 1992). The instrumental positions have been reported onto the absolute coordinate system by adopting the star catalog by Dalessandro et al. (2014) as astrometric reference and by using the cross-correlation software `CataXcorr` (Montegriffo et al. 1995). The instrumental magnitudes of the final catalog have been finally calibrated by using a sample of stars in common with the VVV catalog. The latter has been realized by using the `DAOPHOT` based VVV-SkZ pipeline (Mauro et al. 2013) and reported into the 2MASS photometric and astrometric system (see details in Chené et al. 2012; Moni Bidin et al. 2011; Mauro et al. 2013). We adopted an iterative 2σ - clipping procedure to estimate the calibration equations transforming the instrumental GeMS K_s and J magnitudes into the VVV photometric system. In order to avoid bias, only the brightest stars (with $K_s < 16$ and $J < 16.5$) were used (see Figure 3), yielding a total of about 300 calibration stars in each filter. The r.m.s. of the calibration is ~ 0.02 mag both in J and in K_s.

3. Near-Infrared Color-Magnitude diagrams of NGC 6624

In order to obtain a clear definition of the evolutionary sequences in the CMD, we selected only very well measured stars by imposing a selection in the sharpness parameter. In particular, we divided our sample in 0.5 magnitude-wide bins and for each bin we derived the median value of the sharpness by applying an iterative $2\sigma-$rejection (an example is shown in Figure 4). All the stars satisfying this selection criterion and lying within 6σ from the median are shown in the (K_s, $J-K_s$) and (J, $J-K_s$) CMDs plotted in Figure 5. These are the deepest and highest-quality CMDs in the NIR ever obtained from the ground for this cluster, but quite comparable with those obtained for NGC 6121 with HAWK-I@VLT (Very Large Telescope; Libralato et al. 2014) and for M15 with PISCES@LBT (Large Binocular Telescope; Monelli et al. 2015).

The NIR GEMINI CMDs presented in this study are fully comparable, both in depth and resolution, to the optical ones obtained by using different instruments on board HST,

such as the WFPC2 (Heasley et al. 2000; Dalessandro et al. 2014) and the ACS/HRC (Siegel et al. 2011; Dalessandro et al. 2014). In Figure 5 the red HB at $K_s \sim 13.3$ and a well defined RGB bump at about $K_s \sim 13.55$ are clearly distinguishable. Unfortunately, the stars lying along the brightest portion of the RGB ($K_s < 14.0$) are saturated in all the available images. The MS-TO region is well defined at $K_s \sim 17.5$ and the MS nicely extends for more than 4 magnitudes down to $K_s \sim 21.5$. At odds with Siegel et al. (2011), we find no evidence of a broad sequence located below the cluster MS at bluer colors, which has been interpreted as a background feature, due to a tidal stream of the Sagittarius dwarf galaxy, located behind the cluster along its line of sight. The reason for such a discrepancy is likely ascribable to the relatively small FOV of GSAOI compared to that of the ACS. At $K_s \sim 20$ we clearly identify the so-called MS "knee" (MS-K), a particular feature commonly defined as the reddest MS point in NIR CMDs. This feature is due to the absorption of molecular hydrogen induced by collisions (Bono et al. 2010) and flags the portion of the MS populated by very low-mass stars (with $M < 0.55 M_{\odot}$). Until now, the MS-K has been observed only by using HST optical+NIR images (Milone et al. 2012b, 2014) and a proper combination of HST and MCAO data (MAD@VLT - Moretti et al. 2009; PISCES@LBT - Monelli et al. 2015 and GeMS - Massari et al. 2015; Turri et al. 2015). The detection shown in Figure 5 is the first determination of the MS-K feature in a purely NIR CMD obtained from the ground. The detailed study of this feature and its use as a possible age indicator (Massari et al. 2015; Di Cecco et al. 2015; Bono et al. 2010) will be discussed in a forthcoming paper (S. Saracino et al. 2016, in preparation).

4. Absolute age determination

In this Section we take advantage of the exquisite quality of the CMDs shown in Figure 5 to estimate the age of NGC 6624 by using the luminosity of the MS-TO as an age indicator.

4.1. Isochrone fitting method

In order to derive the age of the cluster via the isochrone fitting method, three main cluster parameters are needed, namely the metallicity, the distance and the reddening.

Metallicity - The most recent metallicity estimate of NGC 6624 is [Fe/H]$= -0.42 \pm 0.07$. This value has been derived indirectly from the new metallicity scale of Carretta et al. (2009, 2010), based on optical high-resolution spectra of about 20 GCs. Other estimates in the literature provide slightly lower metallicities: [Fe/H]$= -0.63$ (Carretta & Gratton 1997,

hereafter CG97; Heasley et al. 2000). Recent high-resolution NIR spectroscopy by Valenti et al. (2011) provides [Fe/H]= -0.69 ± 0.02 and $[\alpha/Fe] \sim +0.39$.

Reddening - $E(B-V)$ color excess estimates in the cluster direction range from 0.25 to 0.33 (Armandroff 1989; Heasley et al. 2000) with a fair agreement on $E(B-V) = 0.28$ (Valenti et al. 2004a; Harris 1996, 2010 edition).

Distance modulus - Different estimates of the distance modulus of NGC 6624 have been obtained: $(m-M)_0 = 14.49$ (Harris 1996, 2010 edition), $(m-M)_0$ =14.40 (Heasley et al. 2000), and $(m-M)_0$ =14.63 (Valenti et al. 2004a).

Both the reddening and the distance modulus were mainly derived in a differential way, by comparing the CMD of NGC 6624 with those of other clusters having the same metallicity and known values of $E(B-V)$ and $(m-M)_0$.

In order to compare theoretical models with the NIR photometry of the cluster, we selected three different sets of α-enhanced isochrones:

1. A Bag of Stellar Tracks and Isochrones (`BaSTI`; Pietrinferni et al. 2004) isochrones with $[\alpha/Fe] = +0.4$, Y = 0.259 and a mass-loss parameter $\eta = 0.4$ (Reimers 1975).

2. Dartmouth Stellar Evolutionary Database (`DSED`; Dotter et al. 2007) isochrones with $[\alpha/Fe] = +0.4$ and Y = 0.2583.

3. Victoria-Regina (`VR`; VandenBerg et al. 2014) isochrones with $[\alpha/Fe] = +0.4$ and Y = 0.2583.

For each model we adopted [Fe/H] = -0.60, a distance modulus of $(m-M)_0 = 14.49$ ($d = 7.9$ Kpc) and a color excess $E(B-V) = 0.28$[4]. These parameters well reproduce the main evolutionary features in the high-quality optical HST CMD by Dalessandro et al. (2014). However, the impact of adopting different values for these parameters will be discussed at the end of this Section.

`BaSTI` *isochrones* - Figure 6 shows a set of seven isochrones with appropriate different ages ranging from 10.5 to 13.5 Gyr, stepped by 0.5 Gyr, overplotted to the data of NGC 6624 in the $(K_s, J-K_s)$ and $(J, J-K_s)$ CMDs, by assuming the quoted distance and reddening. The `BaSTI` NIR colors and magnitudes are on the Johnson-Cousins-Glass photometric system, so they were converted first on the Bessell & Brett (1988) system and then, by using

[4]The color excess in the NIR filters $E(J-K_s)$ has been derived by adopting the extinction coefficients $A_J/E(B-V) = 0.899$ and $A_{K_s}/E(B-V) = 0.366$ from Casagrande & VandenBerg (2014)

the transformations of Carpenter (2001), into the 2MASS photometric system (Cutri et al. 2003).
As can be seen, the agreement between BaSTI models and our data is quite good in the extended MS and in the TO region, while it is not completely satisfactory in terms of color at the level of the MS-K (at $K_s > 19.5$)[5] and in the lower part of the RGB. A mismatch between models and data appears also at the brightest portion of the RGB, at $K_s < 14$ but in this case it is likely due to non-linearity and saturation problems that mainly affect the K_s band photometry. In spite of this, both the luminosity of the RGB bump and the ZAHB level are well reproduced (see Figure 6).

Focussing on the TO region, in order to identify the isochrone that best reproduces the observations, we performed a χ^2 analysis. The χ^2 parameter has been computed by selecting a subsample of stars in the MS-TO region, in the magnitude range $16.4 < K_s < 17.8$, where the isochrone shape is particularly sensitive to age variations. It has been defined as: $\chi^2 = \sum[(O_K - E_K)^2 + (O_{colJK} - E_{colJK})^2]$. We computed, iteratively, the minimum distance both in magnitude (O_K) and in color (O_{colJK}) between each star in our sample and the corresponding values E_K and E_{colJK} read along the isochrone. The result is shown in the right panel of Figure 7. As can be seen, a well defined minimum is visible, indicating a best-fit isochrone with an absolute age of $t_{age} = 12.0 \pm 0.5$ Gyr.

DSED *isochrones* - Following the same approach adopted for the BaSTI isochrones, Figure 8 shows the comparison between the observed cluster photometry and the DSED isochrones (Dotter et al. 2007). A color offset $\delta(J - K_s) = +0.003$ (corresponding to $\delta K_s = -0.003$) was needed to reconcile these evolutionary models to the data, in agreement with what found by Cohen et al. (2015). DSED isochrones do a good job of reproducing the observed CMD morphology of NGC 6624, from the SGB level down to the MS-K. The RGB instead shows the same discrepancies already seen for the BaSTI isochrones, with the only difference that in this case, even the magnitude of the RGB bump is not well reproduced. This is likely due to the fact that different models treat overshooting from convective cores in different ways. A χ^2 test has been performed also for DSED models and the minimum value has been obtained for an absolute age of $t_{age} = 12.0 \pm 0.5$ Gyr. This result is shown in Figure 9, together with a zoom into the MS-TO/SGB regions of NGC 6624.

VR *isochrones* - Finally, the $(K_s, J - K_s)$ and $(J, J - K_s)$ CMDs of NGC 6624 have been compared to the new VR isochrones (VandenBerg et al. 2014) (see Figure 10). According to

[5]However, it should be noted that the BaSTI models do not sample the entire extension of the MS since they are truncated at $M = 0.5 M_{\odot}$.

the results of VandenBerg et al. (2013) and Cohen et al. (2015) we needed to apply a color shift of -0.008 in order to have a good match between models and data. The MS-TO and the SGB level are well reproduced, as well as the shape of the MS-K. At the base of the RGB instead, `VR` models are systematically too red compared with the observed photometry. By performing a χ^2 test on the `VR` isochrones, we obtained a slightly older absolute age of $t_{age} = 12.5 \pm 0.5$ Gyr, however in agreement, within the uncertainties of the method, with the ages derived from `BaSTI` and `DSED` models.

Figures 6, 8 and 10 show that there is a mismatch between all models and observation starting from the RGB base. As discussed in detail by Salaris et al. (2007), Brasseur et al. (2010) and Cohen et al. (2015), this is a well known and long-standing problem. It may be related to some issues depending on the T_{eff} - color transformations in the IR, and possibly caused by uncertainties in the model atmospheres, like treatment of absorption lines as a function of gravity and to the abundance of some specific elements.
The impact of the adopted chemical composition on the overall quality of the fit has been tested. In particular, we compared isochrones with [Fe/H] = -0.42 and [α/Fe] = +0.2 adopted by VandenBerg et al. (2013) for their age derivation of NGC 6624 and [Fe/H] = -0.60 & [α/Fe] = +0.4 that we have used for our age derivation. For a fixed age, the two isochrones ([Fe/H] = -0.60 & [α/Fe] = +0.4 and [Fe/H] = -0.42 & [α/Fe] = +0.2) exactly match, showing only a slight difference at the MS-K level. We have also considered the effect of the abundance variations. Cohen et al. (2015) showed that a modest helium enhancement of Y=0.04 is not able to solve the observed disagreement between models and data at the SGB/RGB level. We verified that the overall match still remains unsatisfactory even adopting isochrones with an helium content as large as Y=0.35. In particular, while the increase of helium results in a better fit at the RGB base, it does not allow to properly reproduce the MS. Finally, we tried to test the impact of adopting different values of reddening and distance on the determination of the age of the cluster. With this aim we performed the same χ^2 analysis as before by assuming the values of Heasley et al. (2000) and Valenti et al. (2004a). This analysis gives age values of 11.0 ± 0.5 Gyr and 10.5 ± 0.5 Gyr respectively. However a visual check reveals that isochrones having such extreme values of E(B-V) and/or $(m - M)_0$ do not reproduce properly the main evolutionary sequences (MS-TO/SGB level, HB level and RGB bump) of the cluster. Hereafter, for our analysis we will adopt the absolute age of 12 Gyr derived from `BaSTI`, the model which better reproduce the overall shape of the CMD of NGC 6624.

4.2. Comparison with previous results

The age of NGC 6624 has been widely debated in recent years. As shown in Figure 12, the value determined in this work is in good agreement, within the errors, with most of the previous estimates quoted in the literature.

The largest discrepancy is found with respect to the value determined by Heasley et al. (2000). By comparing the CMD of NGC 6624 with those of NGC 6637 and 47 Tucanae (having a similar metallicity), the authors established that these clusters have the same age (14 ± 1 Gyr) by using the Yale isochrones. A relatively old age (13.00 ± 0.75 Gyr) was also found by Dotter et al. (2010), analyzing `DSED` models with the following chemical composition: [Fe/H]$= -0.50$ (by assuming the scale by Zinn & West 1984, hereafter ZW84) and [α/Fe]$= 0$. An absolute age of 10.6 ± 1.4 Gyr, in quite good agreement with the one estimated in this work (within their large error bars), was instead obtained by Salaris & Weiss (2002), both for a metallicity of [Fe/H]$= -0.50$ (ZW84 scale) and for [Fe/H]$= -0.70$ (CG97 scale). Meissner & Weiss (2006) derived for NGC 6624 two different ages: 12 Gyr from the model best reproducing the MS-TO region (as in our case), and a lower limit of 10.5 Gyr, from the isochrone providing an acceptable fit to all the investigated age indicators. From the isochrone fitting and the ZAHB loci, VandenBerg et al. (2013) derived the ages of 55 GCs for which the optical HST/ACS photometry was publicly available. In the case of NGC 6624 the absolute age resulted to be 11.25 ± 0.5 Gyr, in good agreement with our value. Finally the most recent study of the cluster was performed by Roediger et al. (2014), within a detailed review on the state of the art about age and metallicity determinations for a sample of 41 Galactic GCs. The authors quote an age of 12.5 ± 0.9 Gyr, which is again consistent with the value obtained in this work.

5. The Luminosity and Mass Function of NGC 6624

We have studied the LF and the MF of MS stars in NGC 6624 and their radial variations within the FOV of GSAOI. This kind of studies has been probed to be an efficient tool to study the effect of cluster internal dynamics on stars in a wide range of masses, including the faint-end of the MS where most of the cluster mass lies. In relaxed systems, the slopes of the MF and LF are expected to vary as a function of the distance from the cluster center, with indexes decreasing as distance increases, because of the different effect of mass segregation. Moreover, the radial variation in the stellar MF of star clusters allow to derive crucial information about the dynamical history of the system (including the amount of mass loss suffered by the clusters, e.g. De Marchi et al. 2007, Vesperini & Heggie 1997) and variation in the stellar initial mass function as recently shown by Webb & Vesperini (2016).

In this context, NGC 6624 is a quite interesting case because it has been classified as a post-core collapse cluster (Trager et al. 1995), hence it has already experienced some of the most energetic and advanced phenomena known to occur during the dynamical evolution of dense stellar systems (Meylan & Heggie 1997).

5.1. Artificial Star Experiment

In order to derive a meaningful MS-LF, it is important to take into account a number of effects (such as blends, photometric errors and stellar crowding) that can limit the photometric accuracy, especially when deriving complete samples of faint stars. In order to assess the impact of these effects, we performed a set of artificial star experiments following the prescriptions reported in Bellazzini et al. (2002b) and Dalessandro et al. (2011, 2015). The main steps of this procedure are briefly summarized below. We initially defined a mean ridge-line (MRL) in the $(K_s, J-K_s)$ plane by considering 0.5 mag-wide bins in K_s and by selecting the corresponding median value in color after a $2\sigma-$clipping rejection (see Table 1 and the red line in Figure 13, left panel). Then, we generated a catalog of simulated stars with a K_s-input magnitude ($K_{s,\rm in}$) extracted from a LF modeled to reproduce the observed LF. To each star extracted from the LF, we finally assigned a J_{in} magnitude by means of an interpolation along the MRL of the cluster. In order to avoid artificially increasing the crowding conditions, only one artificial star was simulated in each run within a 20×20 pixels cell (more than 5 times the typical FWHM of stars on the images). In addition, we imposed each simulated star to have a minimum distance of about 50 pixels from the edges of each chip. By imposing these criteria and adopting the coordinate transformations discussed in Section 2, artificial stars were added to the 13 J and 14 K_s images by using the `DAOPHOT II/ADDSTAR` software. This procedure was performed individually on each chip and the artificial stars thus obtained were analyzed by using the same PSF models and the same reduction process (including the same selection criteria) adopted for the real images, as fully described in Section 2. A total of ~ 48000 artificial stars per chip have been simulated. Figure 13 shows a comparison between the simulated (*left panel*) and the observed CMD (*right panel*). It is quite evident that the two CMDs are fully compatible over the entire magnitude range covered by the observations, in particular the simulated MS (for $K_s > 16$) shows the same spread in color as the observed one, thus confirming that the procedure is fully appropriate.

The artificial star catalog thus obtained was used to derive the completeness curves as the ratio ($\Gamma = N_{\rm out}/N_{\rm in}$) between the number of stars recovered after the photometric reduction ($N_{\rm out}$) and the number of simulated stars ($N_{\rm in}$) in each magnitude bin. The

completeness curves as a function of the K_s magnitudes for three different radial bins ($0'' \leq r < 15''$, $15'' \leq r < 30''$ and $r \geq 30''$, where r is the distance from the cluster center[6]) are shown in Figure 14. This clearly testify to a high (90-100%) photometric completeness of the GEMINI catalog down to $K_s \sim 19 - 20$, depending on the distance from the center.

5.2. Luminosity and Mass functions

In order to derive the MS-LF of NGC 6624 we adopted the radial bins defined for the determination of the completeness curves (see Section 5.1). Starting from the $(K_s, J - K_s)$ CMD, we selected a sample of bona-fide MS stars defined as those stars located within 2.5σ from the MRL, where σ is the combined photometric uncertainty in the K_s and J bands. For each radial interval, we considered only the stars with K_s magnitude ranging between 16 and the value corresponding to a completeness factor $\Gamma \sim 0.5$, namely $K_s = 20.35$ for $0'' \leq r < 15''$, $K_s = 20.45$ for $15'' \leq r < 30''$ and $K_s = 20.55$ for $r \geq 30''$. The observed LF obtained in each radial interval was thus corrected for incompleteness by adopting the appropriate value of Γ in each bin of magnitude. The completeness-corrected LF was then decontaminated from the effect of field stars by using the Besançon simulation of our Galaxy (Robin et al. 2003) for a region of about $2.5'$ squared centered on NGC 6624, rescaled on the GSAOI FOV. For each magnitude bin, the density of field stars has been estimated and then subtracted (see for example Bellazzini et al. 1999). In Figure 15 the completeness-corrected and background-subtracted LFs of NGC 6624 in different radial bins are shown. In order to compare the LFs obtained at different distance from the cluster center, the LFs have been normalized to the one obtained for the innermost region in the magnitude range $16.0 < K_s < 17.5$. The comparison shows that the LFs are clearly different, with the LF in the outer regions of the cluster showing an overabundance of low-luminosity stars with respect to those in the innermost radial bin, consistent with the effect of mass segregation. This is in agreement with results by Goldsbury et al. (2013).

Following a similar approach, we have also derived the MF of NGC 6624. Masses have been estimated from the `BaSTI` isochrone that best-fits the CMD, as discussed in Section 4.1. This provides a MS-TO mass of $0.88 M_{\odot}$. The MF covers a range in mass from $0.9 M_{\odot}$

[6]We recomputed the cluster center $C_{\rm grav}$ of NGC 6624 by applying the algorithm of Casertano & Hut (1985) to evaluate, through an iterative procedure, the "density center" of the stellar positions, i.e. their average position weighted by the local number density (for more details, see Lanzoni et al. 2007, 2010). Using various initial searching radii, ranging from $5''$ to $20''$, and applying a cut in magnitude $K_s = 18$ to avoid incompleteness, we finally found $\alpha_{J2000} = 18^h 23^m 40^s.52$, $\delta_{J2000} = -30°21'40''.25$ with an uncertainty of about $0.2''$.

down to lower limits corresponding to $\Gamma \approx 0.5$: $M = 0.49 M_{\odot}$ for $0'' \leq r < 15''$, $0.47 M_{\odot}$ for $15'' \leq r < 30''$ and $0.45 M_{\odot}$ for $r \geq 30''$. The MFs are shown in Figure 16, with the same color code as in Figure 15 to indicate different distances from the cluster center. We used the MF of the innermost radial bin as a reference and we normalized the more external ones by using the number counts in the mass range $0.8 \leq M/M_{\odot} < 0.9$. As appear in Figure 16 and in agreement with what we obtained from the analysis of the LFs, the MFs show a clear variation of their slopes, flattening moving outwards. Such a trend clearly demonstrates that this cluster has already experienced a significant degree of mass segregation. In general, all GCs are expected to show evidence of mass segregation, because of their short relaxation timescales (e.g. Paust et al. 2010). However, recent results have shown that there are some exceptions: see the case of ω-Centauri (Ferraro et al. 2006a), NGC 2419 (Dalessandro et al. 2008, Bellazzini et al. 2012), Terzan 8 and Arp 2 (Salinas et al. 2012), Palomar 14 (Beccari et al. 2011) and NGC 6101 (Dalessandro et al. 2015). These examples suggest that either some mechanisms able to suppress mass segregation may occur in some GCs or that theoretical relaxation times may suffer of significant uncertainties. In this context, the study of the dynamical state of a cluster becomes quite interesting.

6. Summary & Conclusions

This work is focused on NGC 6624, a metal-rich globular cluster located in the Galactic bulge. By combining the exceptional capabilities of the adaptive optics system GeMS with the high resolution camera GSAOI on the GEMINI South telescope, we obtained the deepest and most accurate NIR $(K_s, J-K_s)$ and $(J, J-K_s)$ CMDs ever obtained from the ground for NGC 6624. The quality of the photometry turns out to be fully competitive with the optical photometry from the HST. The derived CMDs span a range of more than 8 magnitudes, allowing to identify all the well known evolutionary sequences, from the HB level to the MS-TO point down to below the MS-K (detected at $K_s \sim 20$), a feature observed so far only rarely in the optical band and identified for the first time here in a purely infrared CMD. We took advantage of our high-resolution photometry to get an accurate estimate of the absolute age of NGC 6624, which is still quite debated in the literature. By adopting the MS-TO fitting method, we determined an absolute age of about 12.0 ± 0.5 Gyr for the cluster.

Taking advantage of this high-quality sample, we studied the MS-LF and MF at different distances from the cluster center. The level of completeness of the MS sample has been evaluated from artificial star experiments and turns out to be larger than 50% down to $K_s \sim 20.3$ at any distance from the cluster center. The completeness-corrected and field-

decontaminated LFs and MFs show significant signatures of mass segregation. In fact, moving from the innermost region of the cluster to the outskirts, the number of low-mass stars gradually increases compared to high-mass stars. This result confirms that NGC 6624 is a dynamically old cluster, already relaxed.

The data obtained for NGC 6624 clearly show that, under favorable conditions (for example the seeing of the observing night or the NGSs magnitude), the GeMS/GSAOI system is able to provide images with similar spatial resolution and photometric quality as HST in the optical bands.

Appendix A Testing stellar variability with the GeMS/GSAOI system

We could also test the stability and accuracy of the GeMS + GSAOI system in performing stellar variability studies. To do this, we focused on the core of NGC 6624. In this region Deutsch et al. (1999) discovered an exotic object (Star1) which has been classified as a quiescent cataclysmic variable or a LMXB. The optical counterpart to this object, named COM_Star1, has been identified by Dalessandro et al. (2014) to be a star showing a clear sinusoidal light modulation and an orbital period of $P_{orb} \approx 98$ minutes. We identified COM_Star1 in our GEMINI J and K_s images (see Figure 17) by using the coordinates reported by Dalessandro et al. (2014). It appears as a relatively bright star at $K_s \sim 17.76$ and $(J - K_s) \sim 0.69$ outside the MS on the red side (it is marked with a red circle in the top panel of Figure 19). Since the object is visible in all GEMINI images (13 in J and 14 in K_s), we could investigate its variability in the infrared bands. Its light curve (red dots in the *bottom panel* of Figure 19) shows a luminosity variation with an amplitude of ~ 0.2 mag and is well folded with the same period ($P_{orb} = 98$ min) found by Dalessandro et al. (2014). For sake of comparison, the light curve of a genuine MS star (StarB) with comparable luminosity (blue circle in Figure 18) is shown in Figure 19, *bottom panel*. As expected, this star is a "normal" non-variable MS, in fact its light curve does not show any evidence of flux modulation ($\sigma_K = 0.017$ mag).
The constancy of the StarB magnitude despite variation of seeing, airmass and PSF shape in the images, implies that the system is largely stable and it can be used to successfully reveal also very small flux variations (of the order of a few 0.01 mag). This test allow us to conclude that the GeMS/GSAOI system indeed has such a high performance and can be successfully used also for stellar variability studies.

We thank the anonymous referee for the careful reading of the paper, and for the useful comments/suggestions. This research is part of the project *Cosmic-Lab* (http://www.cosmic-lab.eu) funded by the European Research Council under contract ERC-2010-AdG-267675. S.S. acknowledges the *"Marco Polo Project"* of the Bologna University for grant support and the University of Concepción for the warm hospitality during her stay when part of this work has been carried out. D.G. and S.V. gratefully acknowledge support from the Chilean BASAL Centro de Excelencia en Astrofísica y Tecnologías Afines (CATA) grant PFB-06/2007. F.M. gratefully acknowledges the support provided by Fondecyt for project 3140177. L.O. acknowledges the PRIN-INAF 2014 CRA 1.05.01.94.11: "Probing the internal dynamics of globular clusters. The first comprehensive radial mapping of individual star kinematics with the new generation of multi-object spectrographs" (PI: L. Origlia). R.E.C. acknowledges funding from Gemini-CONICYT Project 32140007. C.M.B. acknowledges support from project Fondecyt Regular 1150060. S.S. and E.D. thank Maurizio Salaris for useful discussions and inputs about the stellar evolutionary models.

Table 1: Mean Ridge-Line of NGC 6624 in the $(K_s, J - K_s)$ CMD.

K_s (mag)	$J - K_s$ (mag)
12.413	0.742
12.913	0.737
13.413	0.727
13.913	0.723
14.413	0.714
14.913	0.706
15.413	0.696
15.913	0.680
16.413	0.644
16.913	0.547
17.413	0.519
17.913	0.528
18.413	0.588
18.913	0.709
19.413	0.897
19.913	0.947
20.413	0.937
20.913	0.877
21.413	0.817

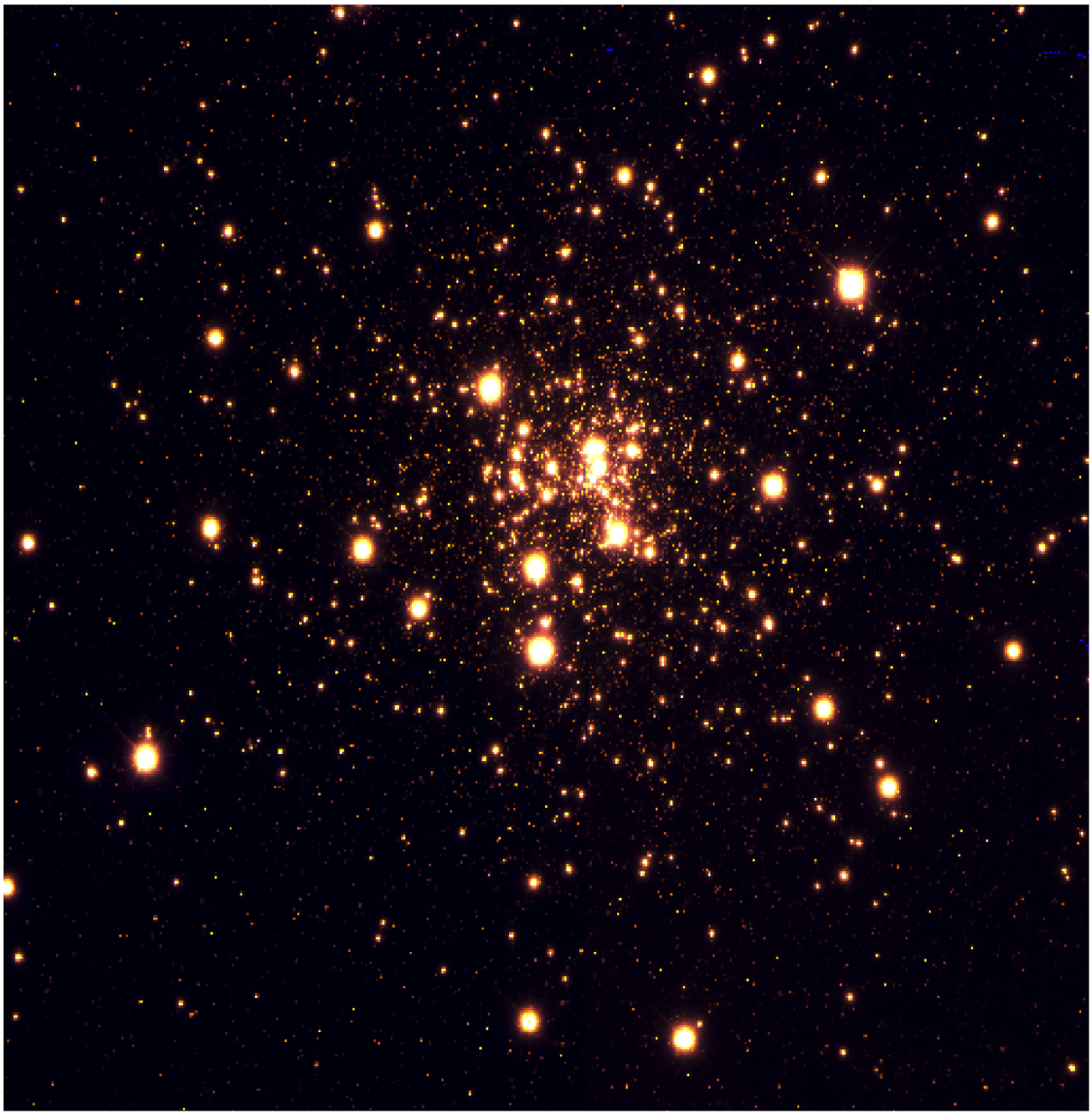

Fig. 1.— Two-color image of NGC 6624 obtained by combining GEMINI observations in the NIR J and K_s bands. North is up, east is on the left. The field of view is $93'' \times 93''$.

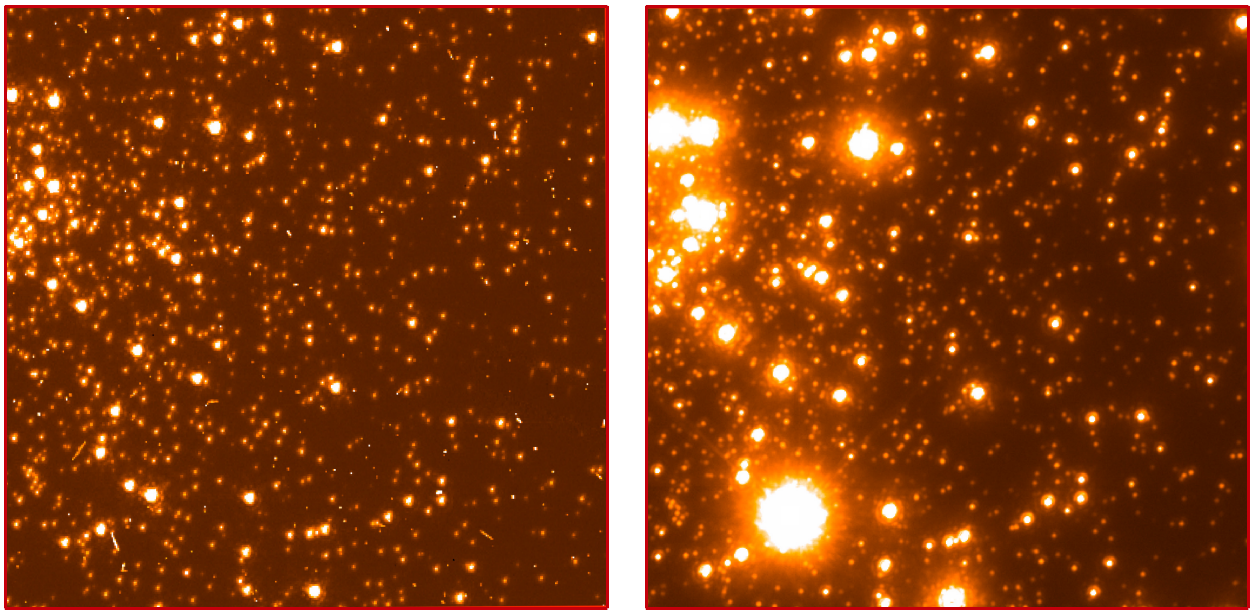

Fig. 2.— A zoom-in of a central region ($10'' \times 10''$) of the cluster as seen by ACS/HRC (F435W filter) on board HST (Dalessandro et al. 2014, *left*) and by GSAOI+GeMS in the K_s band (this work, *right*). The spatial resolution of GEMINI in the NIR turns out to be comparable to that of HST in the optical.

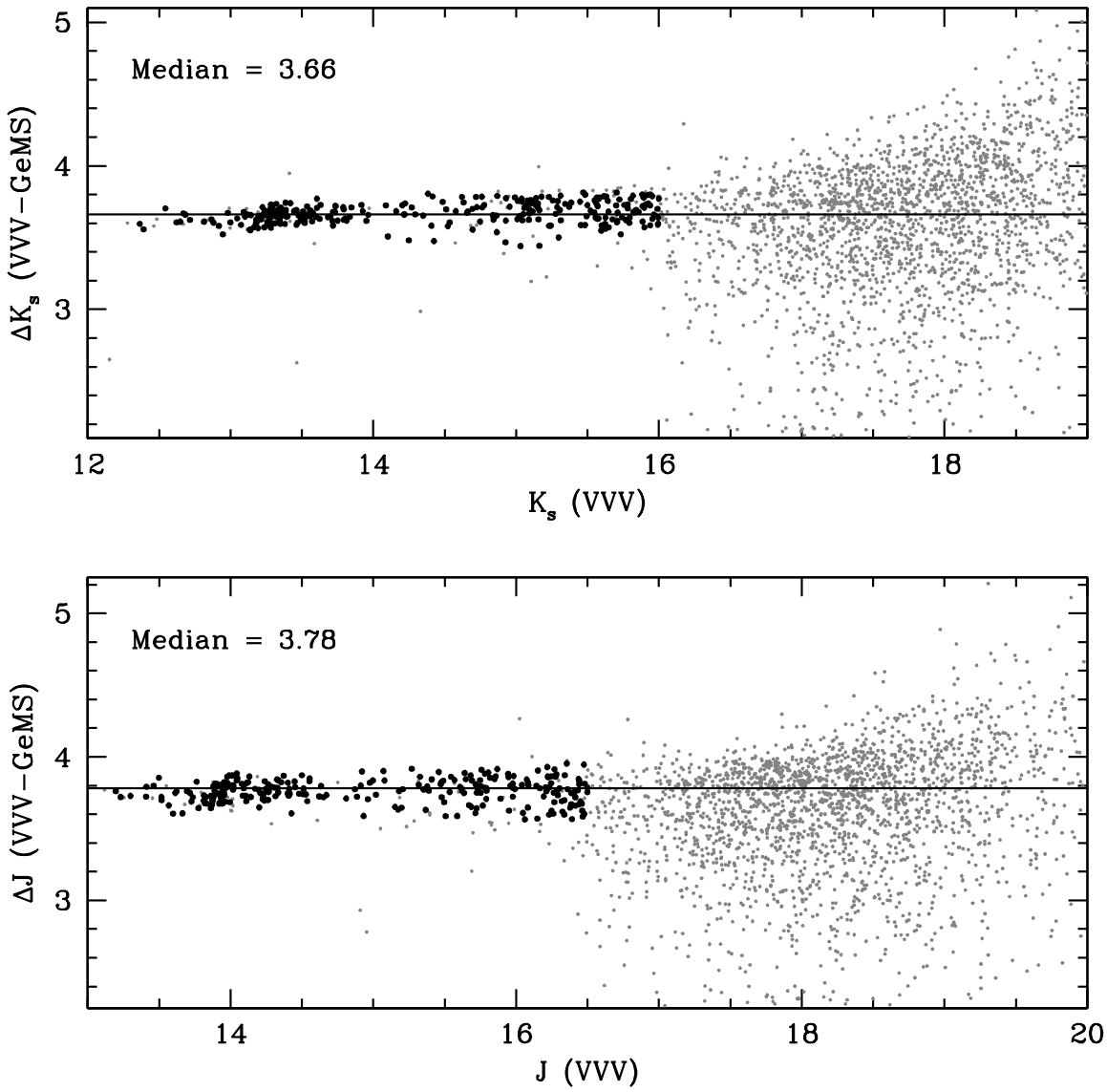

Fig. 3.— Photometric calibration plots for the GEMINI catalog of NGC 6624 in the K_s and J bands. Only bright stars (black points) have been used to determine the calibration zero points. The median values, estimated by using a $2\sigma-$rejection, are shown in the figure.

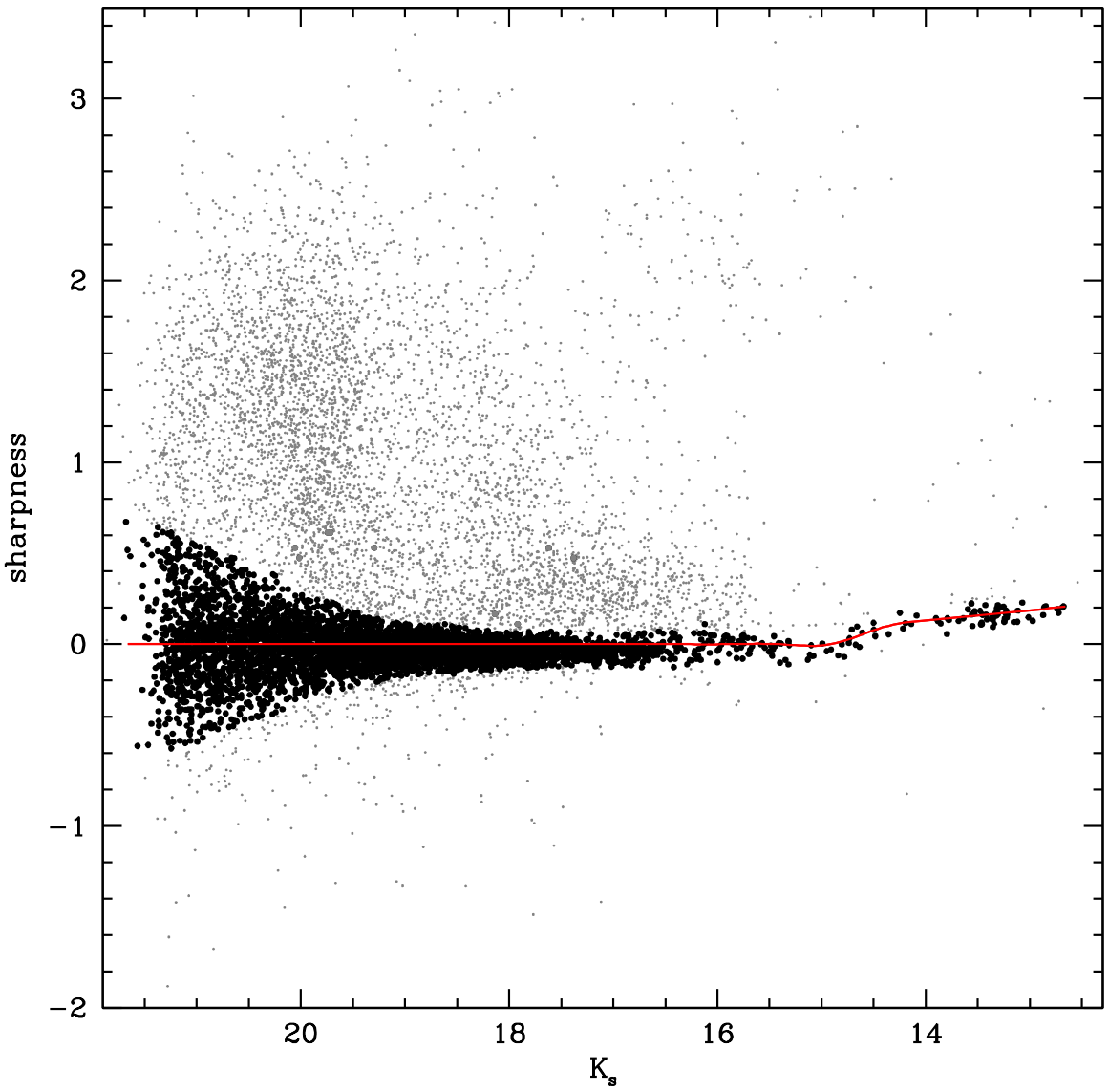

Fig. 4.— Plot of the sharpness as a function of the K_s magnitude. The black points are the stars lying within 6σ from the red line, which represents the 2σ-clipped median value in sharpness. This selection criterion is applied to all the detected stars in order to remove spurious objects and stars with large photometric errors.

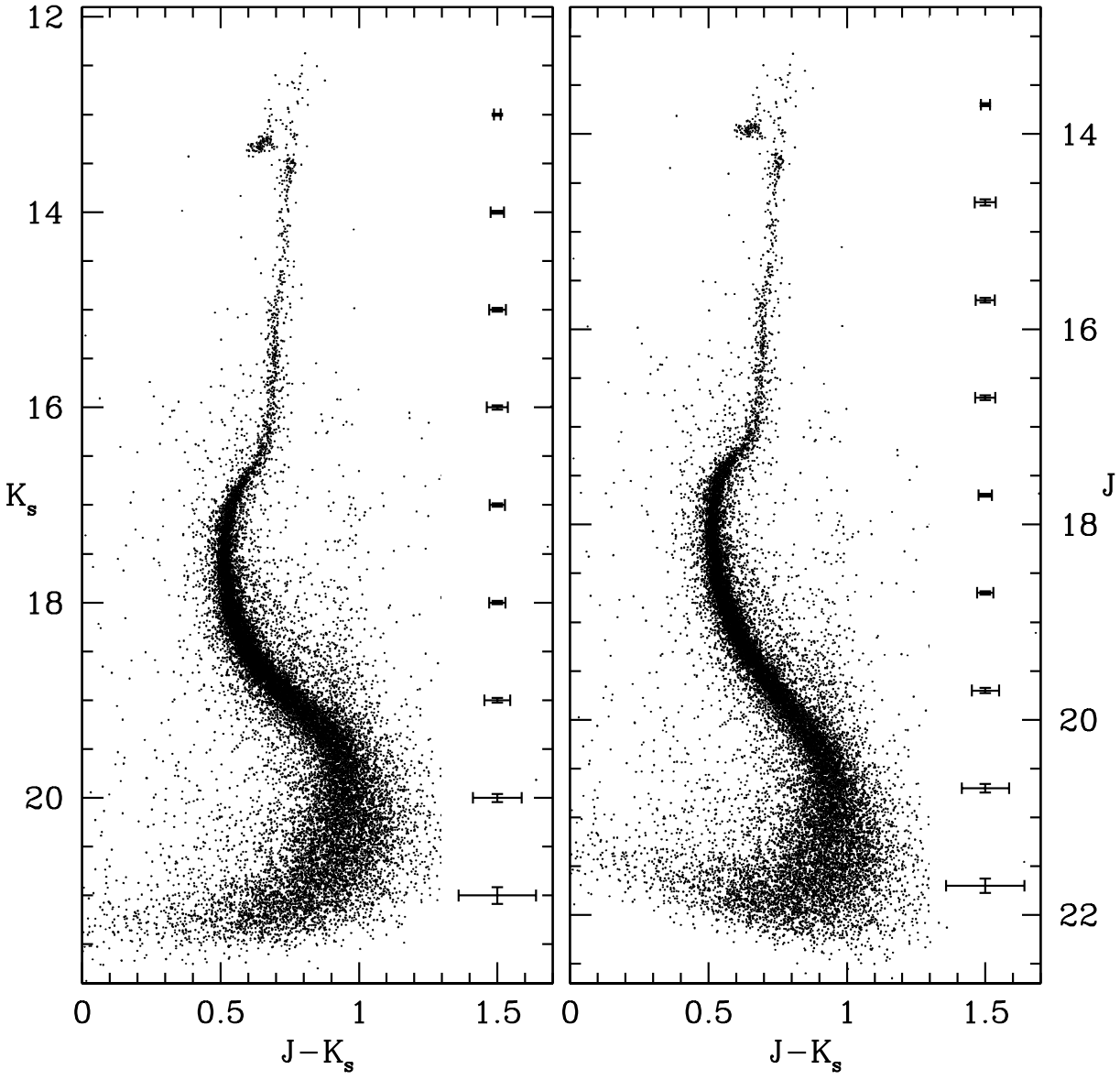

Fig. 5.— $(K_s, J - K_s)$ and $(J, J - K_s)$ CMDs of NGC 6624 obtained from the GEMINI observations discussed in the paper. All the main evolutionary sequences of the cluster are well visible, from the RGB, HB, MS-TO down to the MS-K. These NIR diagrams turn out to be comparable to the HST optical ones, both in depth and in photometric accuracy. The photometric errors for each bin of K_s and J magnitudes are shown on the right side of the panels.

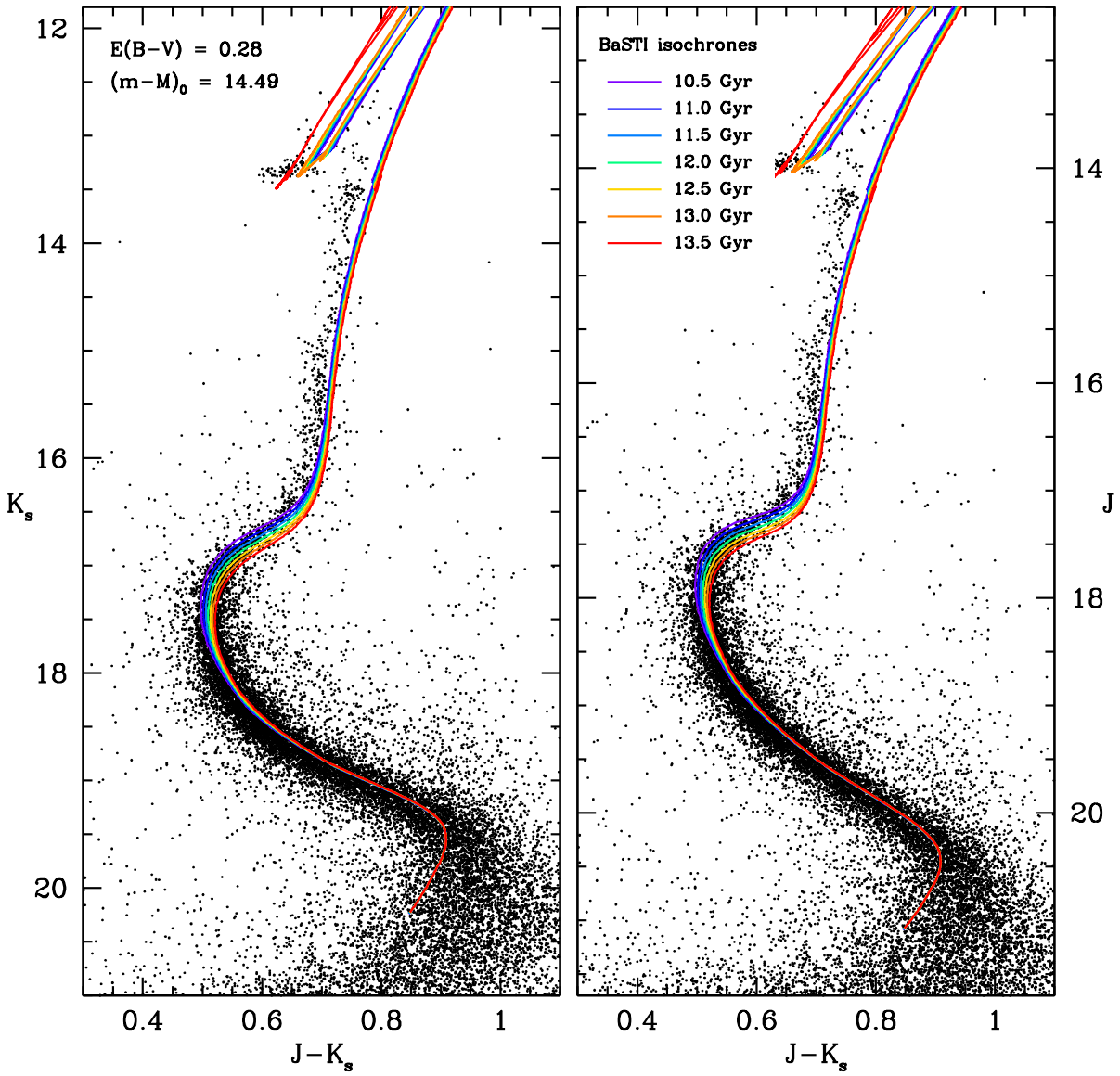

Fig. 6.— $(K_s, J-K_s)$ and $(J, J-K_s)$ CMDs of NGC 6624 CMDs with overplotted a set of `BaSTI` (Pietrinferni et al. 2004) isochrones with ages ranging from 10.5 Gyr up to 13.5 Gyr, in steps of 0.5 Gyr (see labels).

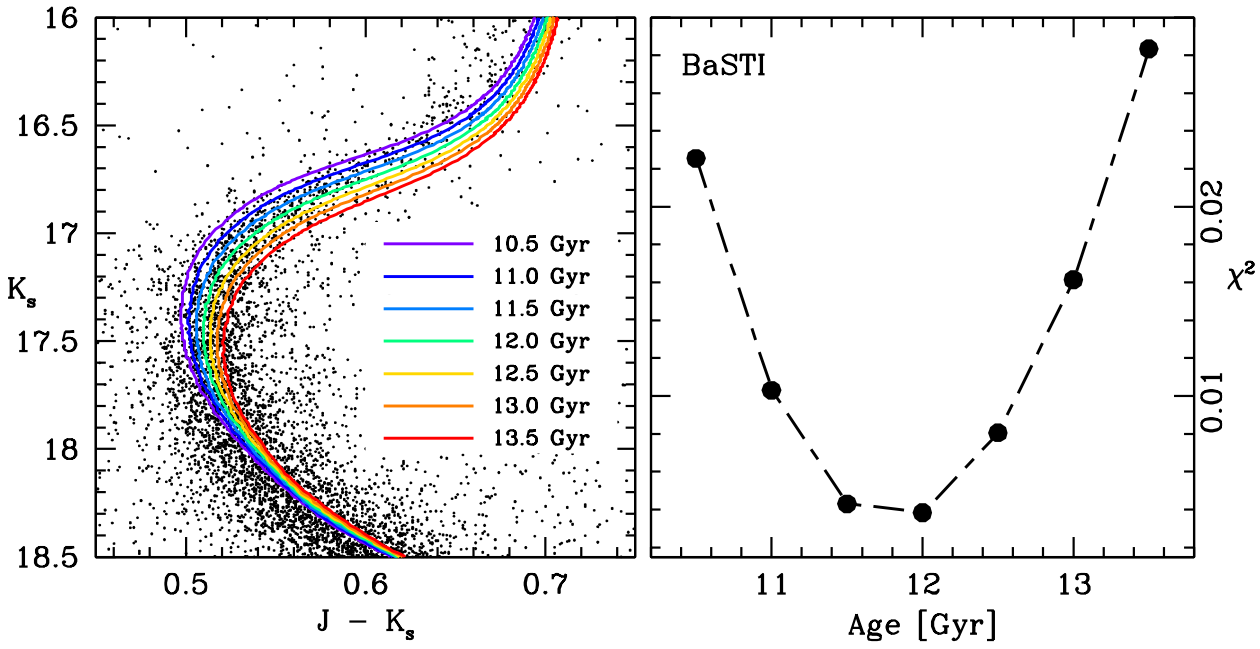

Fig. 7.— *Left panel:* zoomed MS-TO region of the $(K_s, J - K_s)$ CMD, with the selected set of `BaSTI` isochrones (with different ages) overplotted. *Right panel:* χ^2 parameter as a function of isochrone ages considered in the *Left Panel*. A well defined minimum identifies the best-fit isochrone (with $t_{age} = 12.0$ Gyr).

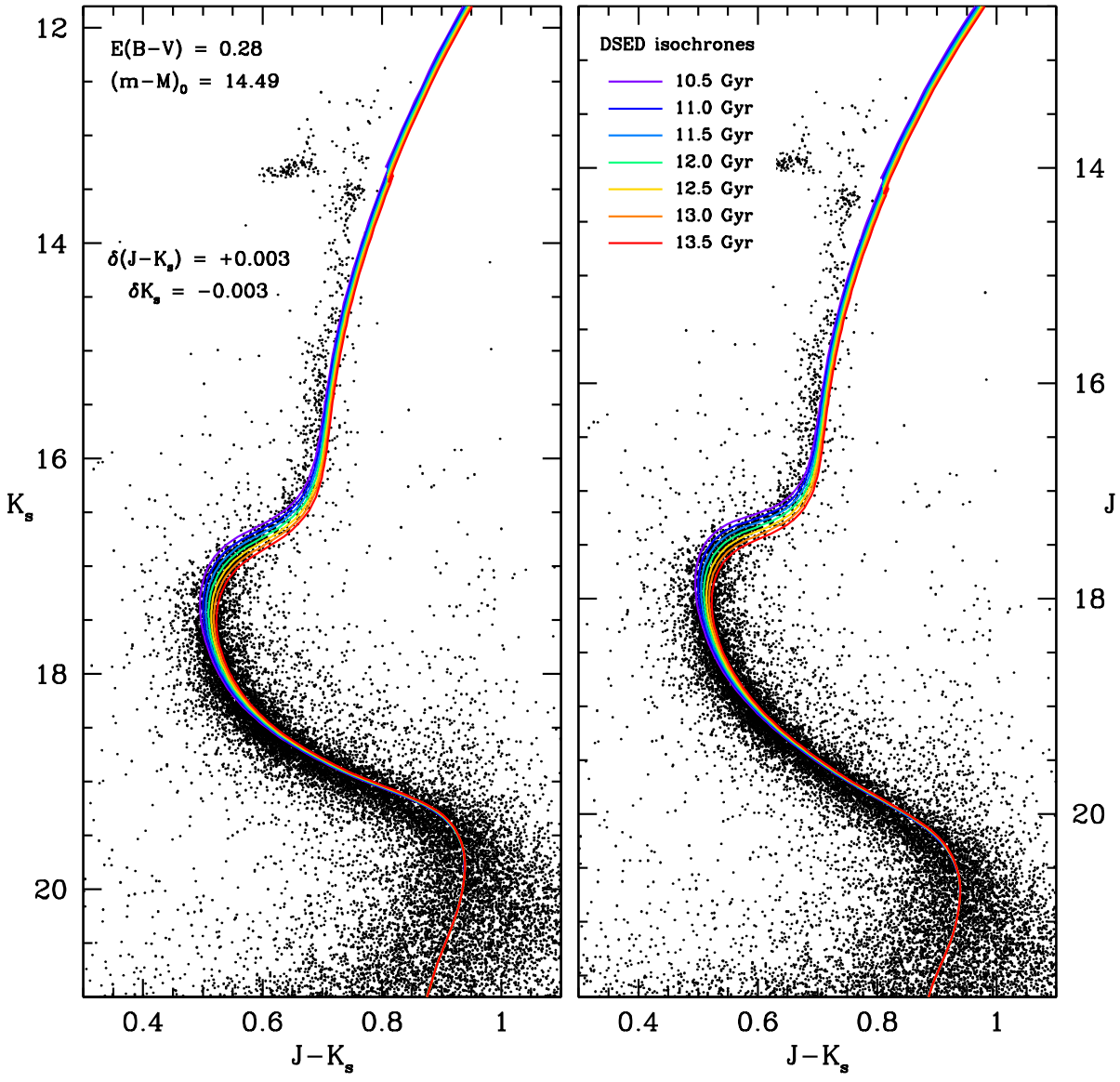

Fig. 8.— The same as in Figure 6 but for DSED isochrones (Dotter et al. 2007).

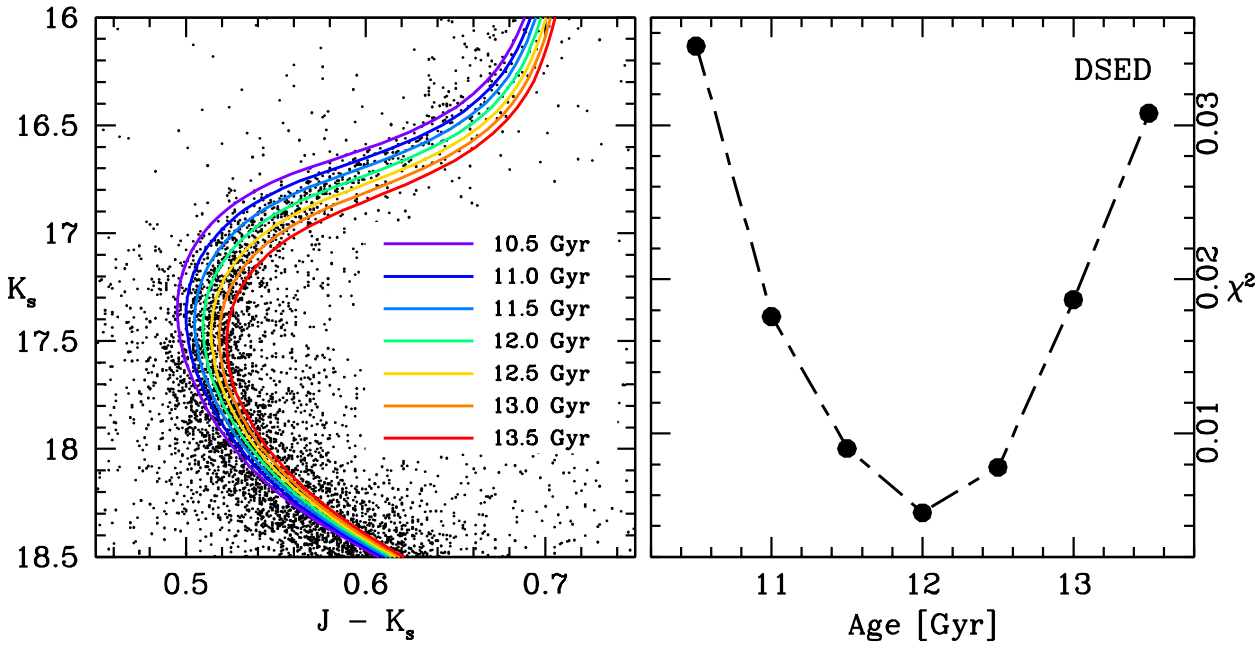

Fig. 9.— The same as in Figure 7 but for DSED isochrones.

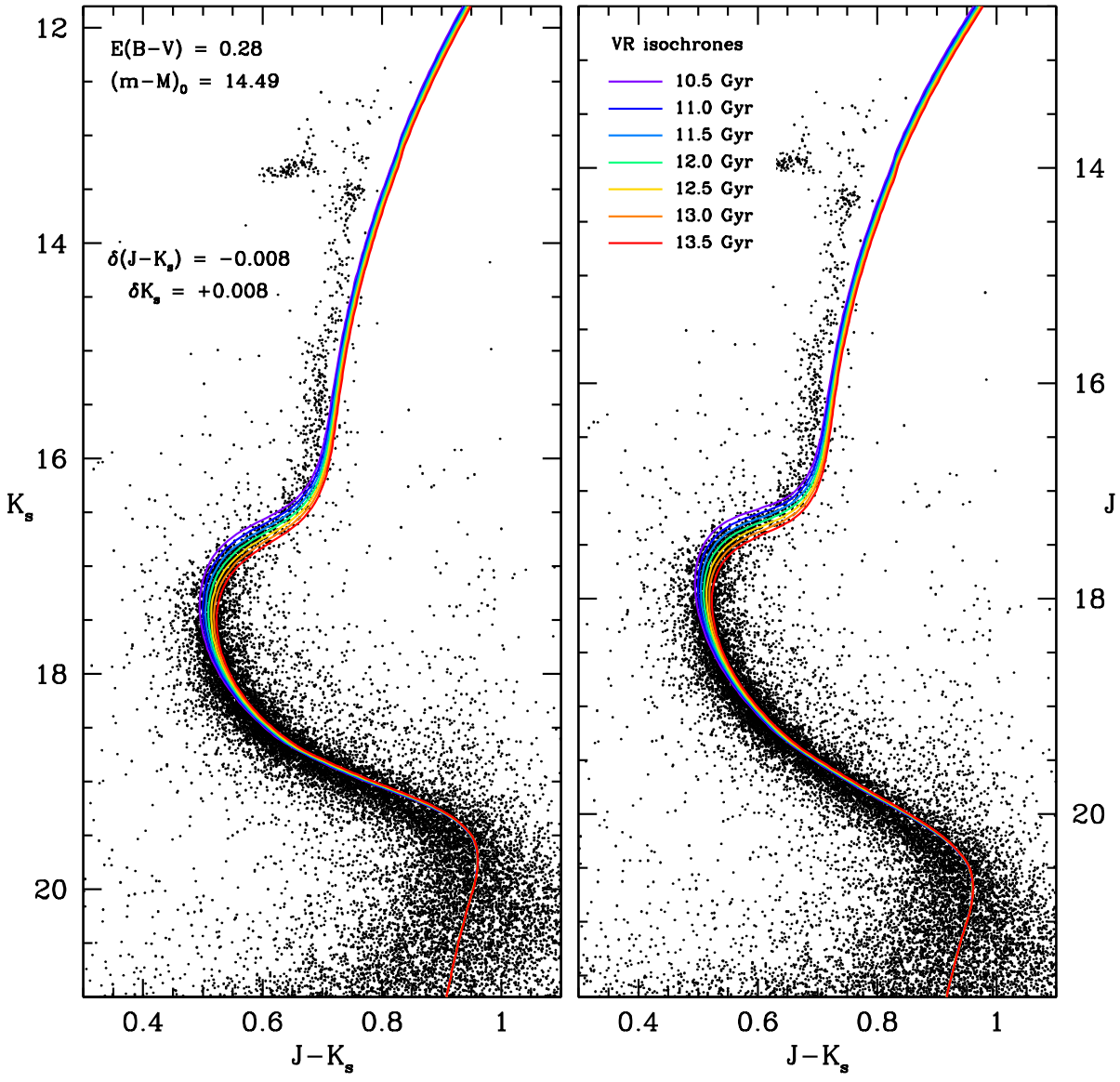

Fig. 10.— The same as in Figure 6 but for VR isochrones (VandenBerg et al. 2014).

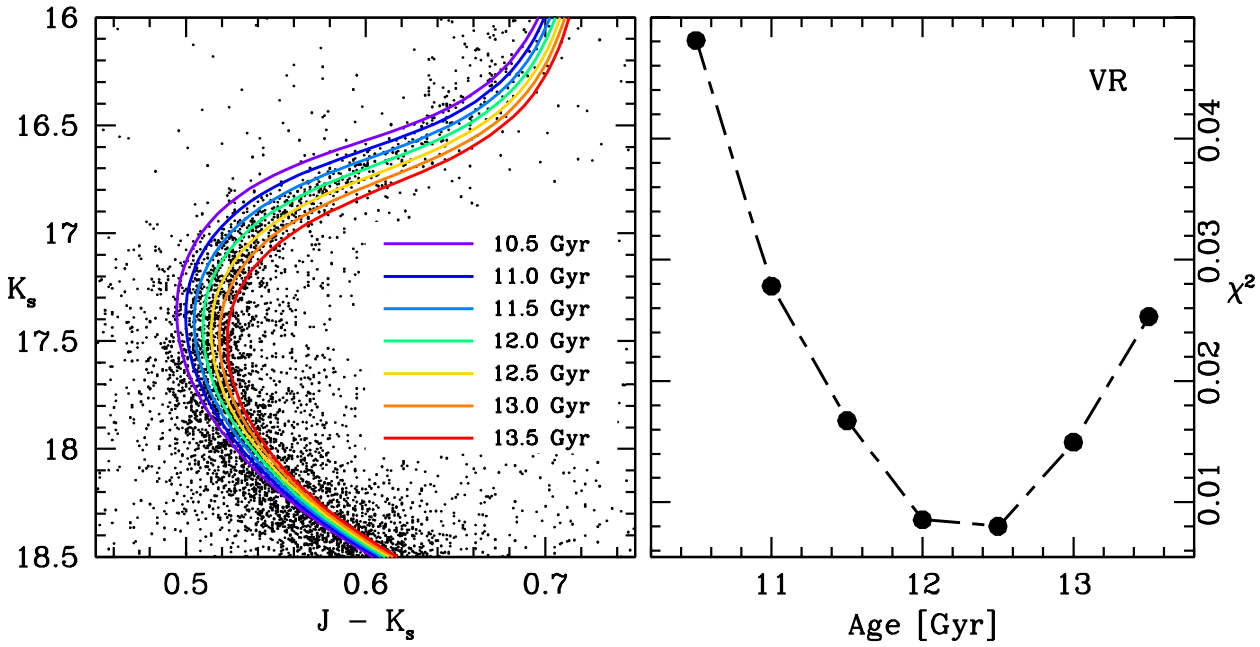

Fig. 11.— The same as in Figure 7 but for VR isochrones.

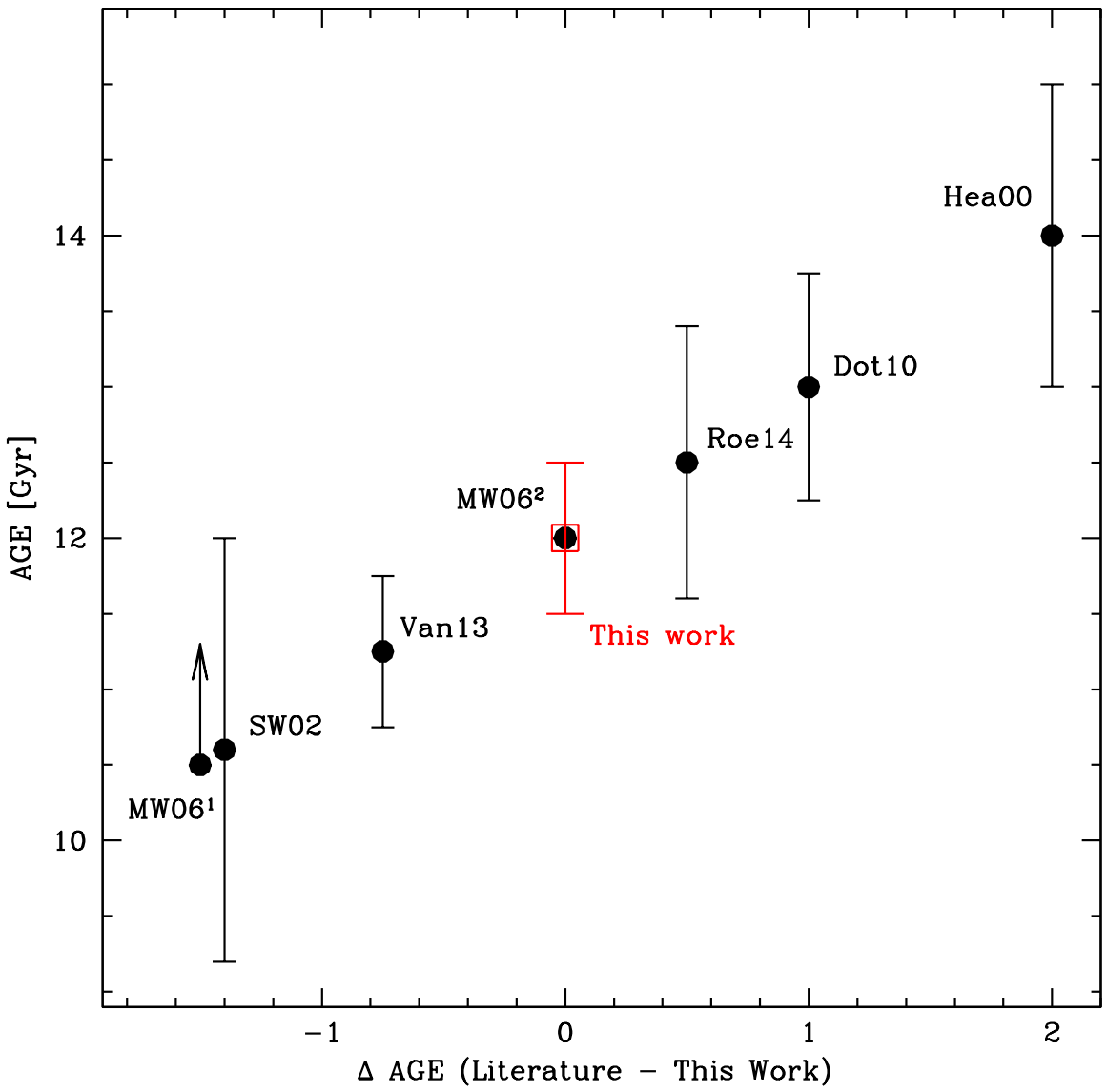

Fig. 12.— Age estimates of NGC 6624 determined in previous studies, compared to that obtained in this work (red point). The acronyms shown in the figure are so defined: **MW06**[1] & **MW06**[2] (Meissner & Weiss 2006), **SW02** (Salaris & Weiss 2002), **Van13** (VandenBerg et al. 2013), **Roe14** (Roediger et al. 2014), **Dot10** (Dotter et al. 2010) and **Hea00** (Heasley et al. 2000).

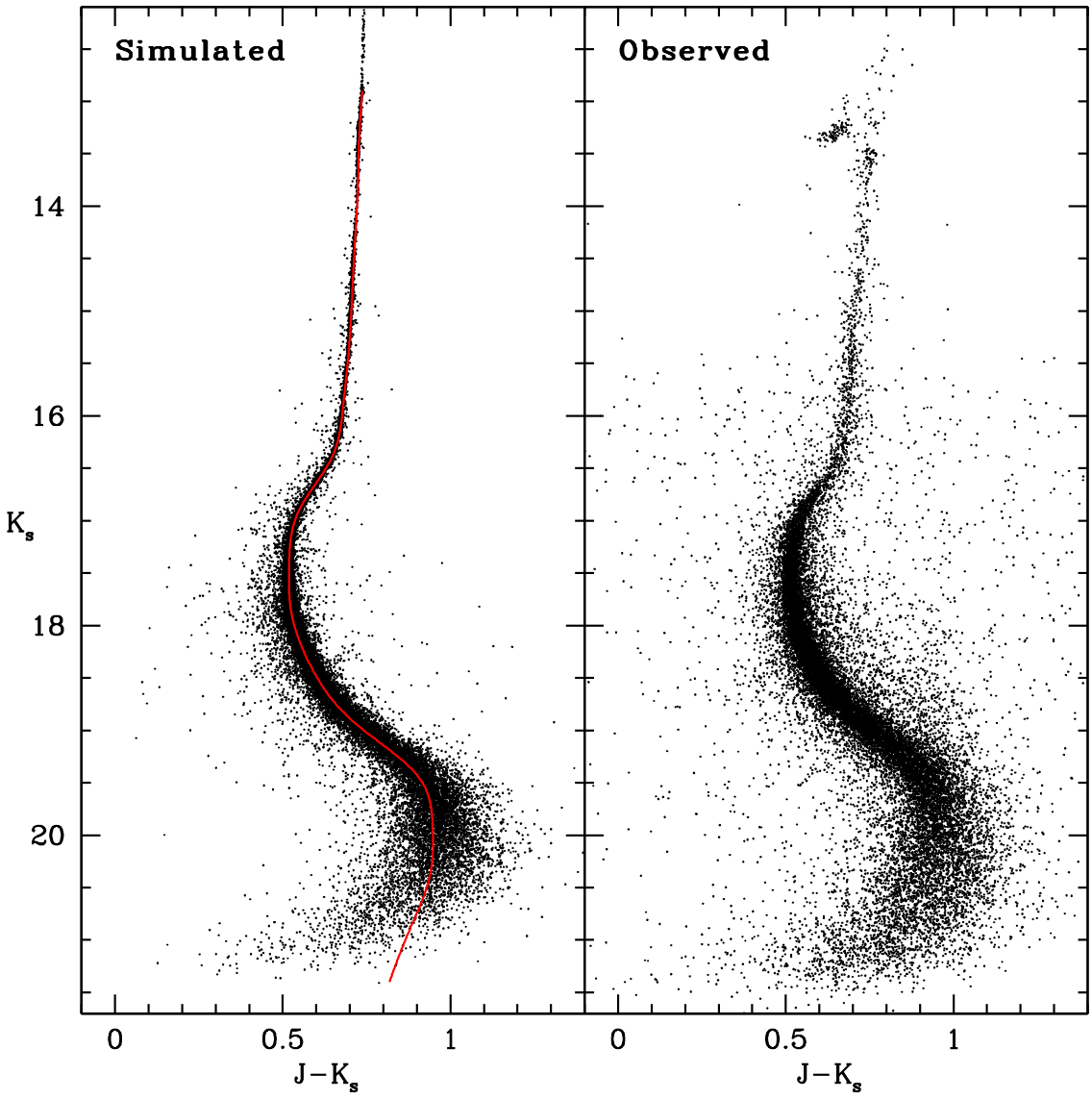

Fig. 13.— Simulated (*left* panel) and observed (*right* panel) $(K_s, J-K_s)$ CMD of NGC 6624, for all the stars that survived the selection: -0.2 $\leq$ sharpness $\leq$ 0.2. As clearly visible, the two CMDs turn out to be fully comparable, especially in the MS region (at $K_s > 16$). The red line in the left panel represents the MRL of NGC 6624 in the $(K_s, J-K_s)$ CMD.

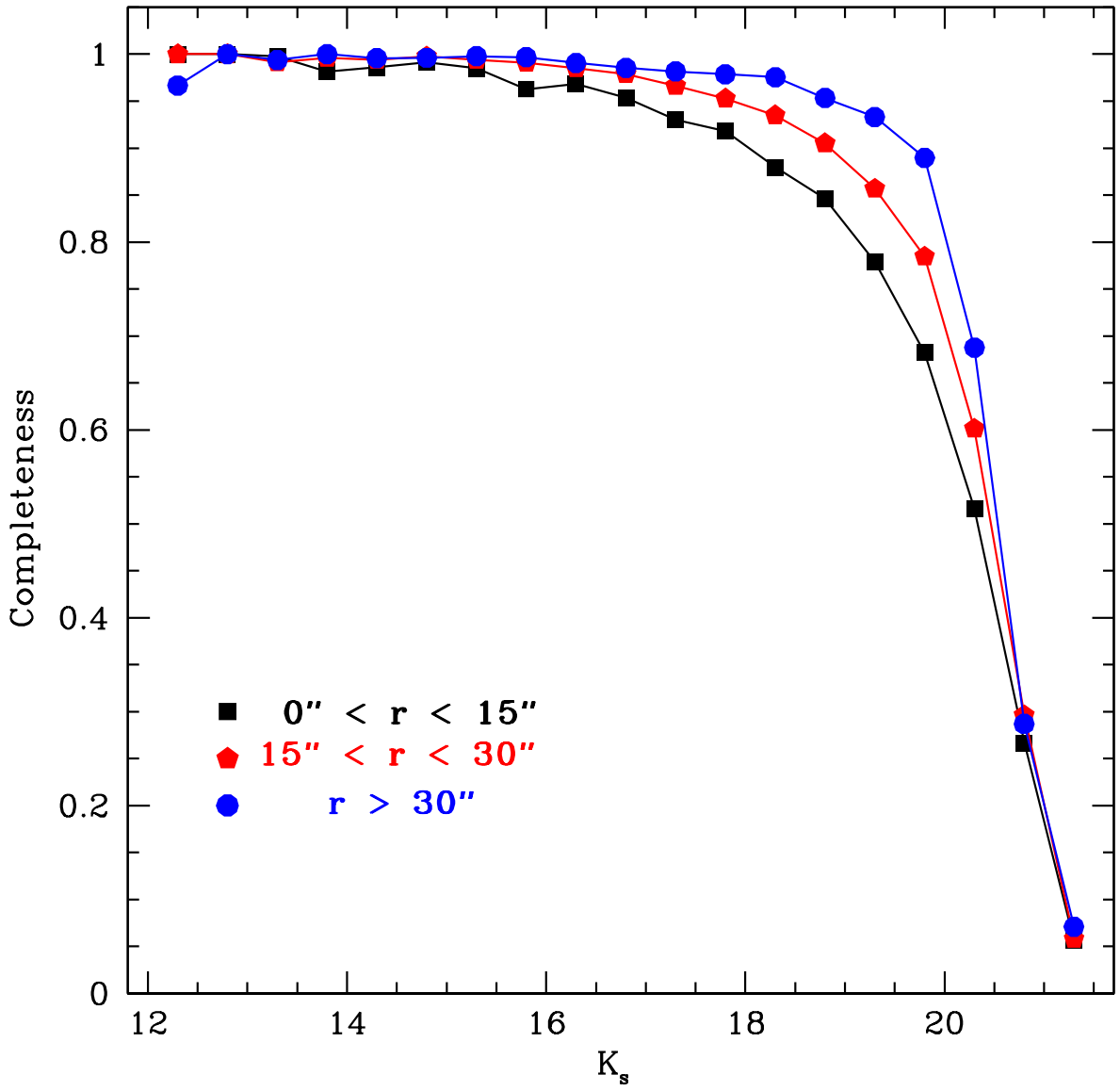

Fig. 14.— Photometric completeness (Γ) as a function of the K_s magnitude for the GEMINI catalog of NGC 6624 in three different radial bins (see labels).

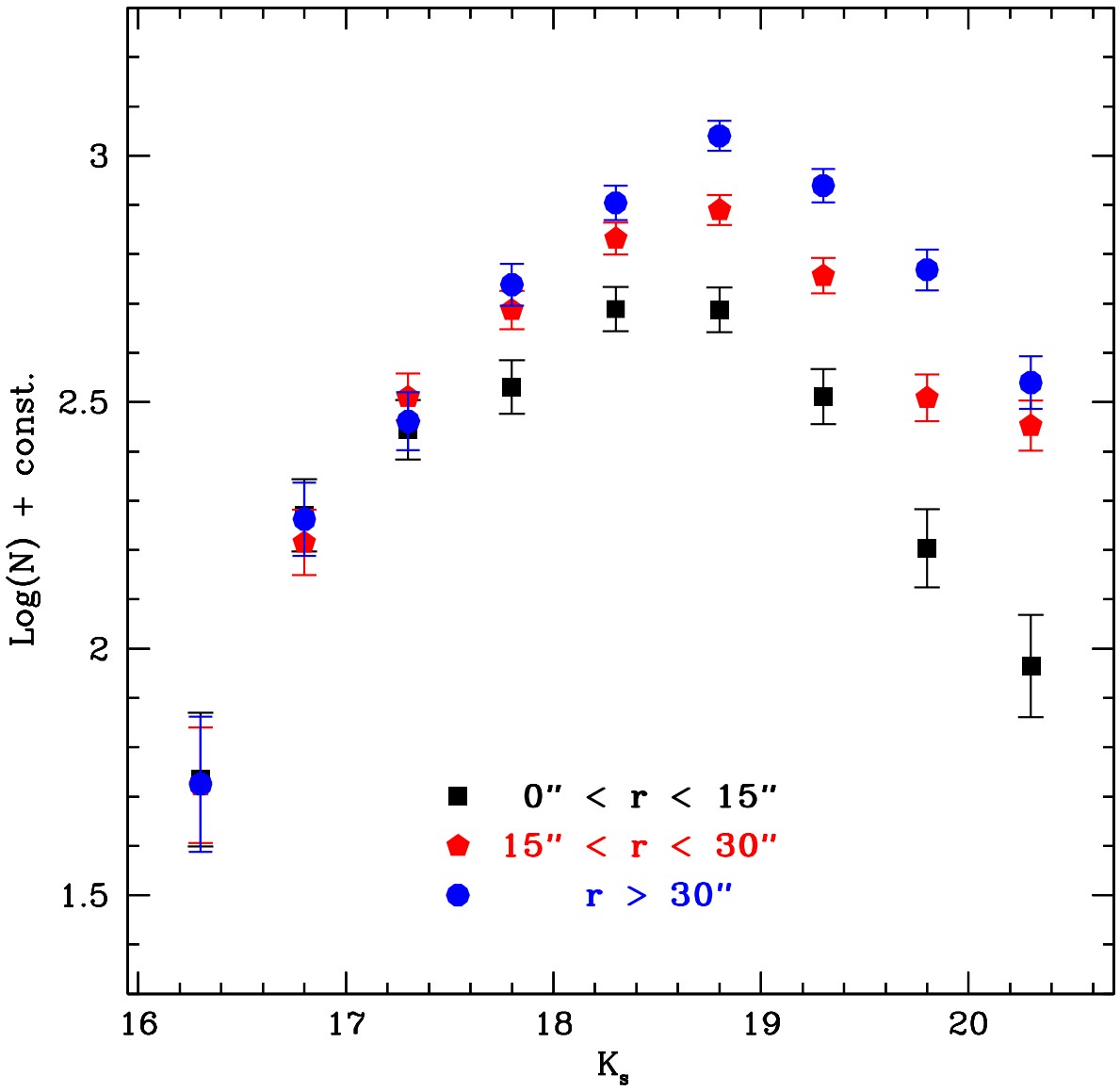

Fig. 15.— NGC 6624 completeness-corrected and field-decontaminated MS-LFs in the K_s band obtained from the GEMINI catalog in three different radial bins. The LF corresponding to the innermost radial bin is used as reference to normalize those at larger radii at the brightest bin.

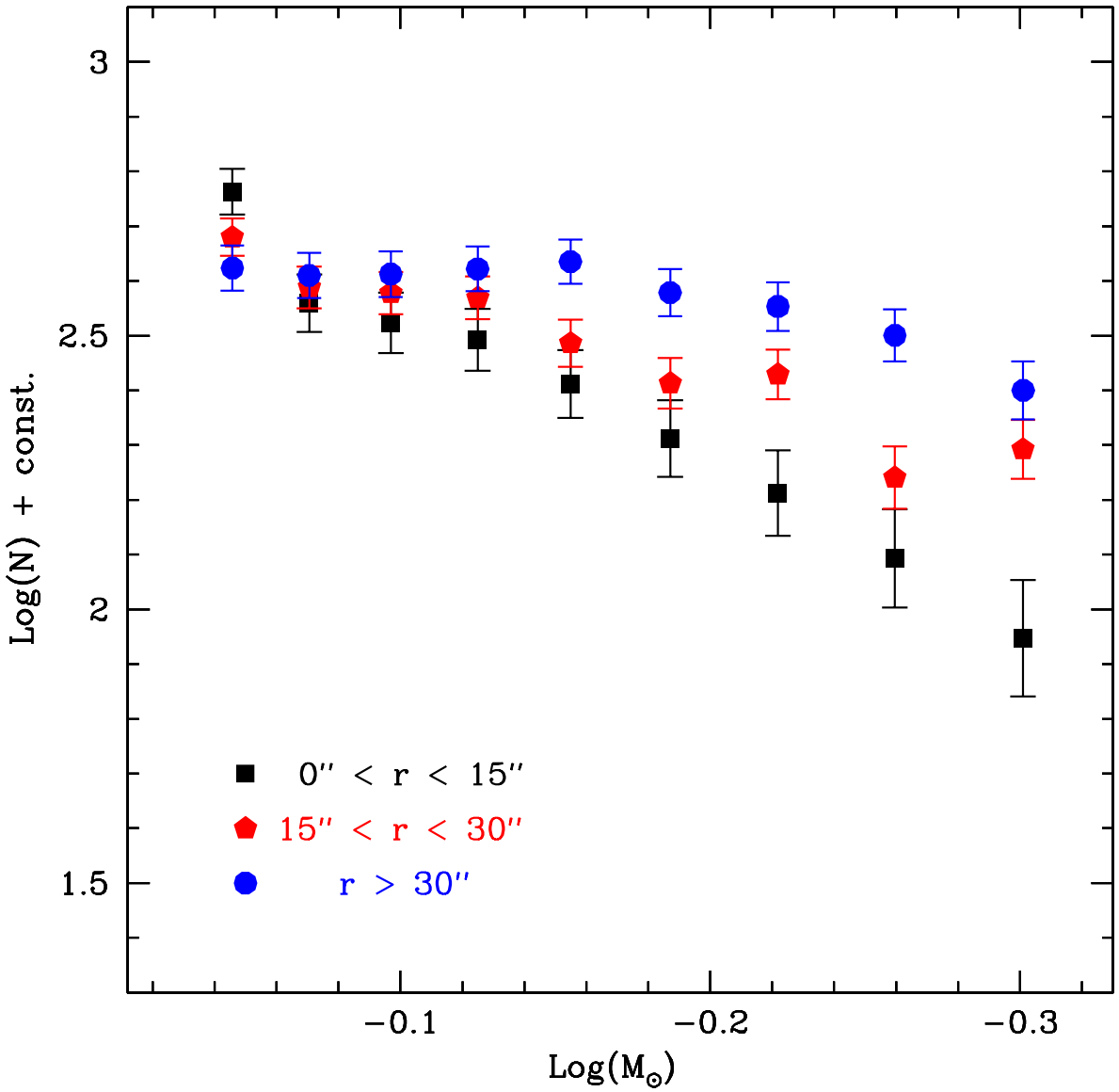

Fig. 16.— MFs derived by using a BaSTI isochrone with [Fe/H] = -0.60 and t_{age} = 12.0 Gyr (see Section 4.1). Radial bins, symbols and colors are the same as in Figure 15.

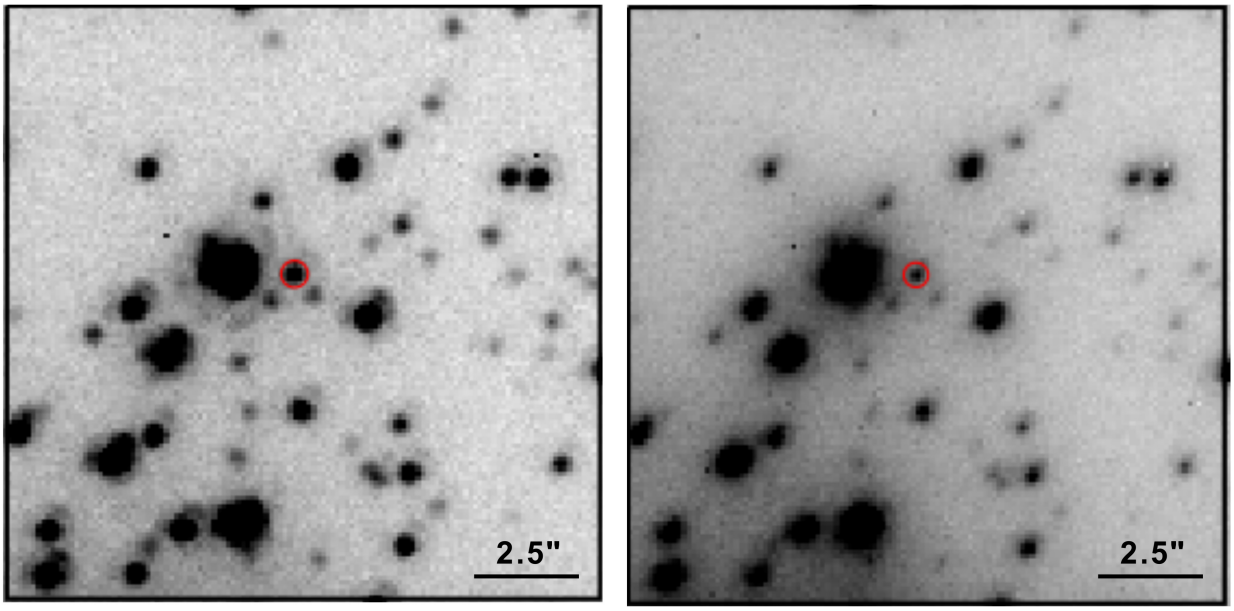

Fig. 17.— *Left panel*: K_s image of a region of $(2.5'' \times 2.5'')$ of NGC 6624, centered on the position of ComStar1, marked with a red circle, as observed by the GeMS/GSAOI system. *Right panel*: The same, but for the J band.

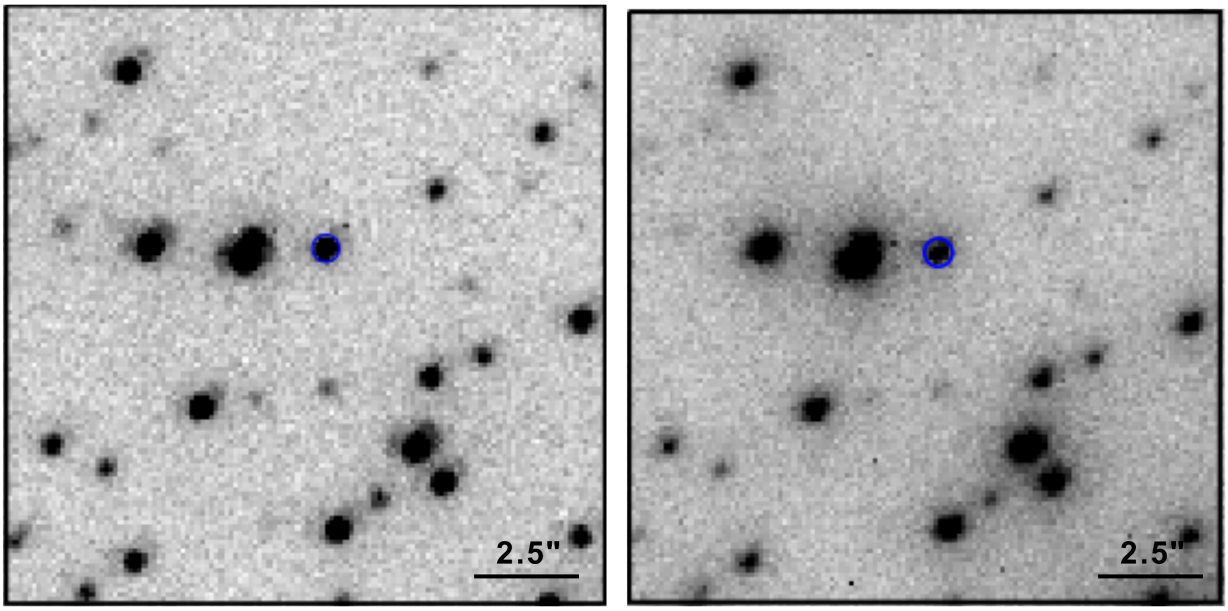

Fig. 18.— *Left panel*: K_s image of a region of $(2.5'' \times 2.5'')$ of NGC 6624, centered on the position of StarB, marked with a blue circle, as observed by the GeMS/GSAOI system. This star has the same magnitude as ComStar1 and is adopted for a comparison. *Right panel*: The same, but in the J band.

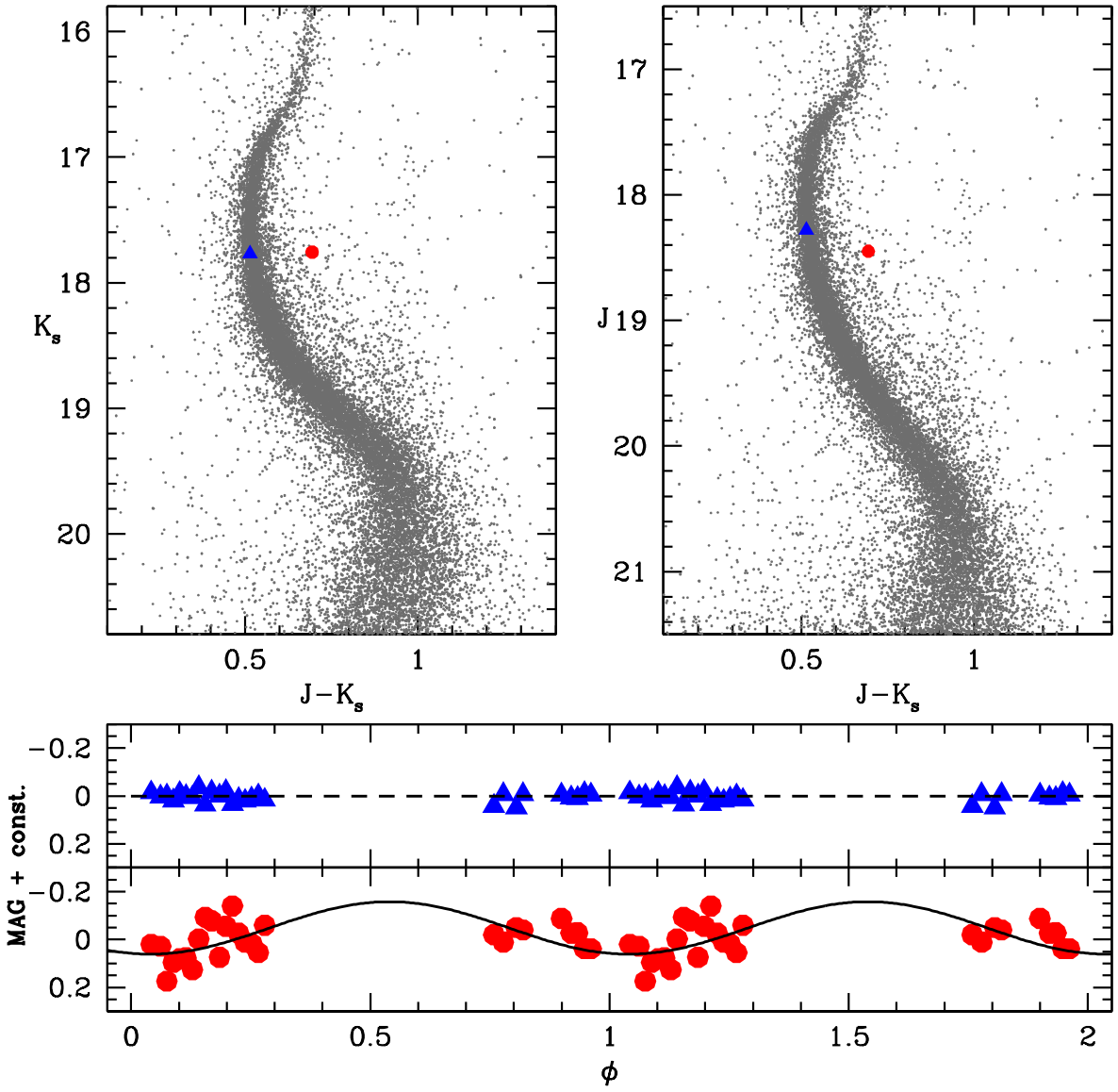

Fig. 19.— *Top panels*: Positions in the $(K_s, J-K_s)$ and $(J, J-K_s)$ CMDs of ComStar1 and StarB are highlighted with a red circle and a blue triangle, respectively. *Bottom panels*: The red circles represent the light curve of ComStar1 folded with the estimated orbital period $P_{orb} \approx 98$ min (Dalessandro et al. 2014). The black line is a sinusoidal function of amplitude ≈ 0.2. For comparison the blue triangles show the light curve of StarB, that has the same average K_s magnitude of ComStar1 but does not show any evidence of flux modulation (dashed black line).

REFERENCES

Armandroff, T. E. 1989, AJ, 97, 1532

Bailyn, C. D. 1992, ApJ, 392, 519

Beccari, G., Pasquato, M., De Marchi, G., et al. 2010, ApJ, 713, 194

Beccari, G., Sollima, A., Ferraro, F. R., et al. 2011, ApJ, 737, L3

Bellazzini, M., Ferraro, F. R., & Buonanno, R. 1999, MNRAS, 307, 619

Bellazzini, M., Fusi Pecci, F., Montegriffo, P., et al. 2002b, AJ, 123, 2541

Bellazzini, M., Dalessandro, E., Sollima, A., & Ibata, R. 2012, MNRAS, 423, 844

Bessell, M. S., & Brett, J. M. 1988, PASP, 110, 1134

Bono, G., Stetson, P. B., VandenBerg, D. A., et al. 2010, ApJ, 708, L74

Brasseur, C. M., Stetson, P. B., VandenBerg, D. A., et al. 2010, AJ, 140, 1672

Cardelli, J. A., Clayton, G. C., & Mathis, J. S. 1989, ApJ, 345, 245

Carpenter, J. 2001, AJ, 121, 2851

Carretta, E., & Gratton, R. G. 1997, A&AS, 121, 95

Carretta, E., Bragaglia, A., Gratton, R., D'Orazi, V., & Lucatello, S. 2009, A&A, 508, 695

Carretta, E., Bragaglia, A., Gratton, R. G., et al. 2010, A&A, 516, A55

Casagrande, L., & VandenBerg, D. A. 2014, MNRAS, 444, 392

Casertano, S., & Hut, P. 1985, ApJ, 298, 80

Catelan, M., Minniti, D., Lucas, P. W., et al. 2011, RR Lyrae Stars, Metal-Poor Stars, and the Galaxy, 145

Chené, A.-N., Borissova, J., Clarke, J. R. A., et al. 2012, A&A, 545, AA54

Cutri, R. M., Skrutskie, M. F., van Dyk, S., et al. 2003, "The IRSA 2MASS All-Sky Point Source Catalog, NASA/IPAC Infrared Science Archive.

Cohen, R. E., Hempel, M., Mauro, F., et al. 2015, AJ, 150, 176

Dalessandro, E., Lanzoni, B., Ferraro, F. R., et al. 2008, ApJ, 681, 311-319

Dalessandro, E., Lanzoni, B., Beccari, G., et al. 2011, ApJ, 743, 11

Dalessandro, E., Pallanca, C., Ferraro, F. R., et al. 2014, ApJ, 784, L29

Dalessandro, E., Ferraro, F. R., Massari, D., et al. 2015, ApJ, 810, 40

Davies, R., & Kasper, M. 2012, ARA&A, 50, 305

De Marchi, G., Paresce, F., & Pulone, L. 2007, ApJ, 656, L65

Deutsch, E. W., Margon, B., Anderson, S. F., & Downes, R. A. 1999, AJ, 118, 2888

Dib, R., Ransom, S. M., Ray, P. S., Kaspi, V. M., & Archibald, A. M. 2005, ApJ, 626, 333

Di Cecco, A., Bono, G., Prada Moroni, P. G., et al. 2015, AJ, 150, 51

Diolaiti, E., Arcidiacono, C., Bregoli, G., et al. 2014, Proc. SPIE, 9148, 91480Y

Dotter, A., Chaboyer, B., Jevremović, D., et al. 2007, AJ, 134, 376

Dotter, A., Sarajedini, A., Anderson, J., et al. 2010, ApJ, 708, 698

Ferraro, F. R., Clementini, G., Fusi Pecci, F., & Buonanno, R. 1991, MNRAS, 252, 357

Ferraro, F. R., Clementini, G., Fusi Pecci, F., Sortino, R., & Buonanno, R. 1992, MNRAS, 256, 391

Ferraro, F. R., Montegriffo, P., Origlia, L., & Fusi Pecci, F. 2000, AJ, 119, 1282

Ferraro, F. R., D'Amico, N., Possenti, A., Mignani, R. P., & Paltrinieri, B. 2001, ApJ, 561, 337

Ferraro, F. R., Sollima, A., Rood, R. T., et al. 2006, ApJ, 638, 433

Ferraro, F. R., Valenti, E., & Origlia, L. 2006, ApJ, 649, 243

Ferraro, F. R., Beccari, G., Dalessandro, E., et al. 2009a, Nature, 462, 1028

Ferraro, F. R., Dalessandro, E., Mucciarelli, A., et al. 2009b, Nature, 462, 483

Ferraro, F. R., Lanzoni, B., Dalessandro, E., et al. 2012, Nature, 492, 393

Freire, P. C. C., Abdo, A. A., Ajello, M., et al. 2011, Science, 334, 1107

Goldsbury, R., Heyl, J., & Richer, H. 2013, ApJ, 778, 57

Harris, W. E. 1996, AJ, 112, 1487

Heasley, J. N., Janes, K. A., Zinn, R., et al. 2000, AJ, 120, 879

Kuchinski, L. E., & Frogel, J. A. 1995, AJ, 110, 2844

Lanzoni, B., Dalessandro, E., Ferraro, F. R., et al. 2007, ApJ, 668, L139

Lanzoni, B., Ferraro, F. R., Dalessandro, E., et al. 2010, ApJ, 717, 653

Libralato, M., Bellini, A., Bedin, L. R., et al. 2014, A&A, 563, A80

Lynch, R. S., Freire, P. C. C., Ransom, S. M., & Jacoby, B. A. 2012, ApJ, 745, 109

Marín-Franch, A., Aparicio, A., Piotto, G., et al. 2009, ApJ, 694, 1498

Massari, D., Fiorentino, G., McConnachie, A., et al. 2015, arXiv:1512.03194

Mauro, F., Moni Bidin, C., Chené, A.-N., et al. 2013, Rev. Mexicana Astron. Astrofis., 49, 189

Meissner, F., & Weiss, A. 2006, A&A, 456, 1085

Meylan, G., & Heggie, D. C. 1997, A&A Rev., 8, 1

Milone, A. P., Marino, A. F., Cassisi, S., et al. 2012, ApJ, 754, L34

Milone, A. P., Marino, A. F., Bedin, L. R., et al. 2014, MNRAS, 439, 1588

Minniti, D., Lucas, P. W., Emerson, J. P., et al. 2010, New A, 15, 433

Moffat, A. F. J. 1969, A&A, 3, 455

Monelli, M., Testa, V., Bono, G., et al. 2015, arXiv:1507.08845

Moni Bidin, C., Mauro, F., Geisler, D., et al. 2011, A&A, 535, AA33

Montegriffo, P., Ferraro, F. R., Fusi Pecci, F., & Origlia, L. 1995, MNRAS, 276, 739

Moretti, A., Piotto, G., Arcidiacono, C., et al. 2009, A&A, 493, 539

Neichel, B., Rigaut, F., Vidal, F., et al. 2014, MNRAS, 440, 1002

Origlia, L., Ferraro, F. R., Fusi Pecci, F., & Oliva, E. 1997, A&A, 321, 859

Origlia, L., Rood, R. T., Fabbri, S., et al. 2007, ApJ, 667, L85

Origlia, L., Rood, R. T., Fabbri, S., et al. 2010, ApJ, 718, 522

Origlia, L., Rich, R. M., Ferraro, F. R., et al. 2011, ApJ, 726, LL20

Origlia, L., Ferraro, F. R., Fabbri, S., et al. 2014, A&A, 564, A136

Paresce, F., de Marchi, G., & Ferraro, F. R. 1992, Nature, 360, 46

Paust, N. E. Q., Reid, I. N., Piotto, G., et al. 2010, AJ, 139, 476

Penny, A. J. 1976, Sussex: University, 1976

Pietrinferni, A., Cassisi, S., Salaris, M., & Castelli, F. 2004, ApJ, 612, 168

Pooley, D., & Hut, P. 2006, ApJ, 646, L143

Ransom, S. M., Hessels, J. W. T., Stairs, I. H., et al. 2005, Science, 307, 892

Reimers, D. 1975, Memoires of the Societe Royale des Sciences de Liege, 8, 369

Renzini, A., & Fusi Pecci, F. 1988, ARA&A, 26, 199

Rigaut, F., Neichel, B., Boccas, M., et al. 2014, MNRAS, 437, 2361

Robin, A. C., Reylé, C., Derrière, S., & Picaud, S. 2003, A&A, 409, 523

Roediger, J. C., Courteau, S., Graves, G., & Schiavon, R. P. 2014, ApJS, 210, 10

Salaris, M., & Weiss, A. 2002, A&A, 388, 492

Salaris, M., Held, E. V., Ortolani, S., Gullieuszik, M., & Momany, Y. 2007, A&A, 476, 243

Salinas, R., Jílková, L., Carraro, G., Catelan, M., & Amigo, P. 2012, MNRAS, 421, 960

Saracino, S., Dalessandro, E., Ferraro, F. R., et al. 2015, ApJ, 806, 152

Sarajedini, A., Bedin, L. R., Chaboyer, B., et al. 2007, AJ, 133, 1658

Siegel, M. H., Majewski, S. R., Law, D. R., et al. 2011, ApJ, 743, 20

Stetson, P. B. 1987, PASP, 99, 191

Stetson, P. B. 1994, PASP, 106, 250

Tam, P. H. T., Kong, A. K. H., Hui, C. Y., et al. 2011, ApJ, 729, 90

Trager, S. C., King, I. R., & Djorgovski, S. 1995, AJ, 109, 218

Turri, P., McConnachie, A. W., Stetson, P. B., et al. 2015, ApJ, 811, L15

Valenti, E., Ferraro, F. R., & Origlia, L. 2004a, MNRAS, 351, 1204

Valenti, E., Ferraro, F. R., & Origlia, L. 2004b, MNRAS, 354, 815

Valenti, E., Ferraro, F. R., & Origlia, L. 2007, AJ, 133, 1287

Valenti, E., Origlia, L., & Rich, R. M. 2011, MNRAS, 414, 2690

VandenBerg, D. A., Brogaard, K., Leaman, R., & Casagrande, L. 2013, ApJ, 775, 134

VandenBerg, D. A., Bergbusch, P. A., Ferguson, J. W., & Edvardsson, B. 2014, ApJ, 794, 72

Vesperini, E., & Heggie, D. C. 1997, MNRAS, 289, 898

Webb, J.J., & Vesperini, E., 2016, MNRAS, in press, arXiv:1608.07293

Zinn, R., & West, M. J. 1984, ApJS, 55, 45

This preprint was prepared with the AAS LaTeX macros v5.2.